UNITED STATES
NAVAL POSTGRADUATE SCHOOL

THESIS

A SCANNING FABRY PEROT INTERFEROMETER
FOR
LASER MODE ANALYSIS
by
John Whitaker Newell

A SCANNING FABRY PEROT INTERFEROMETER

FOR

LASER MODE ANALYSIS

* * * * *

John Whitaker Newell

A SCANNING FABRY PEROT INTERFEROMETER

FOR

LASER MODE ANALYSIS

by

John Whitaker Newell

Lieutenant, United States Navy

Submitted in partial fulfillment of
the requirements for the degree of

MASTER OF SCIENCE

IN

ENGINEERING ELECTRONICS

United States Naval Postgraduate School

Monterey, California

1 9 6 5

A SCANNING FABRY PEROT INTERFEROMETER

FOR

LASER MODE ANALYSIS

by

John Whitaker Newell

This work is accepted as fulfilling
the thesis requirements for the degree of

MASTER OF SCIENCE
IN
ENGINEERING ELECTRONICS

from the

United States Naval Postgraduate School

Vladislav Bevc
Faculty Advisor

Charles H Rothauge
Chairman
Department Electrical
Engineering

Approved: R. E. Wildell
Academic Dean

ABSTRACT

A high resolution scanning Fabry Perot interferometer was constructed for the purpose of spectral analysis of gas laser radiation. The performance of the interferometer is evaluated and a finesse in excess of 250 is noted. Matching requirements and alignment procedures for application of the scanning interferometer are summarized. The results of application of the interferometer to engineering problems and laboratory measurements including visual display of laser modes, determination of frequency stability and frequency drift, and studies of the FM Laser system are reported. High resolution photographs of typical FM Laser spectra are presented showing a 10 to 1 improvement over previous results in the program, thus emphasizing the value of such an interferometer to state of the art developments in optical communications.

ACKNOWLEDGEMENTS

This work was performed at the Electronic Defense Laboratories, Sylvania Electronic Systems, in Mountain View, California. The author expresses grateful appreciation for the supervision, assistance and encouragement of Dr. Burton Mc Murtry and his staff of the Optics Research Department, Sylvania throughout the project. The advice and confidence of Professor Vladislav Bevc of the U. S. Naval Postgraduate School and his patient assistance with this presentation is acknowledged with deep appreciation. The technical assistance of Mr. Lyle Wishart of Sylvania, who assembled the interferometer, is acknowledged with pleasure.

TABLE OF CONTENTS

LIST OF ILLUSTRATIONS

Table of Symbols and Abbreviations

c	velocity of light
λ	wavelength
ν	frequency
μ	index of refraction
δ	phase shift per path
α	fractional power loss per reflection
R,T,A	Fresnel reflection, transmission and absorbtion coefficients
A_i,A_t	Light amplitudes, incident and transmitted
I_i,I_t	Light intensities, incident and transmitted
$\mathcal{F}$	interferometer finesse
$2\Delta\nu$	interferometer half-intensity width
f	focal length of a lens or lens combination
f_c	focal length of lens used for beam collimation
f_o	characteristic matching length parameter
L	separation of reflectors in an optical resonator
R_c	radius of curvature of a spherical mirror
w	beam radius, general
w_o	minimum beam radius, general
w_L	beam radius for the laser
w_I	beam radius for the interferometer
w_1	minimum beam radius for the laser
w_2	minimum beam radius for the interferometer

d	distance, in a matching situation
q	axial mode number
m,n	transverse mode numbers
S_i	piezoelectric strain tensor component
d_{ij}	piezoelectric deformation tensor component
E_j	electric field

1. Introduction

A. General background and purpose

High resolution spectral analysis of laser radiation utilizing the output of gas lasers of the type suggested by Schalow and Townes [1] and initially realized experimentally with a mixture of He-Ne gasses by Javan and co-workers [2], has become increasingly important as progress is made toward the development of working optical communications systems. [3] Detailed knowledge of the relative amplitudes, phases, number and distribution of the laser modes [4,5,6] is both valuable and necessary in such specialized studies as optical heterodyning techniques, [7,8] where carrier and local oscillator frequency characteristics must be well defined and controlled. To understand and achieve controllable single frequency generation while maintaining adequate output power, it is important to observe carefully the structure and behavior of the laser mode spectrum during experimentation. This is best emphasized by recent work on the development and application of the FM Laser concept, [9,10,11] where the effect of internal modulation on the laser output must be studied closely to determine accurate parameters and develop means for reliable mode control [12] for communication requirements.

The value of the application of a scanning Fabry Perot interferometer [13,14](henceforth abbreviated SFPI) to spectral analysis and study of laser radiation has recently been emphasized by Fork, Herriot and Kogelnik [15]. The SFPI method provides visual information of high resolution about the mode spectrum of laser radiation. Studies of mode spectra of laser radiation utilizing the combination of photomixing and RF

beat frequency spectrum analysis [16] are now complemented and in many instances surpassed by the SFPI method which provides a direct high resolution display of the radiation spectral characteristics.

B. Outline of the Thesis

During a ten week association with the Optics Research Department, Electronics Defense Labratories of the Sylvania Electronics Systems in Mountain View, California, the author constructed and evaluated a high resolution scanning Fabry Perot interferometer. This interferometer was then applied to the study of Spectra Physics models 131 and 115 laser[1] outputs while free running, and to the study of the spectral characteristics of the FM Laser during experimentation in that program.

Sections 2 and 3 present the basic theory of the interferometer light transmitting characteristics and the alignment and matching requirements to obtain experimental results of the high resolution desired. Sections 4 and 5 describe the interferometer construction and the results of the experimental evaluation completed. Section 6 describes a brief application of the SFPI to the study of laser frequency stability characteristics. The FM Laser concept is discussed in Section 7 and an operating system including the application of the SFPI is described. Finally, high resolution photographs of typical FM laser output spectra are presented and compared with previous results of Harris and Targ [9] to emphasize the value of the SFPI to this and many other possible studies of laser radiation characteristics.

[1]Spectra Physics Corp. Mountain View, California Data Sheet Nos. SP1008A-5M1064 and SP1007B-5M1064

2. Characteristics of the Scanning Fabry Perot Interferometer

A. Transmitted light amplitude for the Fabry Perot Interferometer

The formula for transmitted light amplitude for the Fabry Perot interferometer is: [17]

$$\frac{A_t}{A_i} = \frac{T e^{i\delta}}{1 - R e^{i2\delta}} \tag{1}$$

The following notation is used:

T and R	Fresnel light intensity transmission and reflection coefficients
A_t and A_i	transmitted and incident light vector amplitudes
$\delta = \frac{2\pi\mu L}{\lambda}\cos\Theta$	phase shift per single traversal

with:

μ	index of refraction
L	separation of the reflectors
λ	wavelength of incident light
Θ	angle formed by the incident light beam with the normal to the reflector surface

Intensity of the transmitted light is given by the Airy's formula:

$$\frac{I_t}{I_i} = \frac{A_t A_t^*}{A_i A_i^*} = \frac{T^2}{(1-R)^2 + 4R\sin^2\delta} \tag{2}$$

This formula is more often written in the form:

$$\frac{I_t}{I_i} = \frac{1}{1 + F\sin^2\delta} \tag{3}$$

where:

$$F = \frac{4R}{(1-R)^2} \tag{4}$$

with T = 1-R.

A modification of the expression for transmitted light intensity is necessary for instances when the reflection coefficient R is greater than 0.99. Scattering and absorbtion losses in the multiple dielectric

coatings of the mirrors must then be included.

Equation (3) is then written:

$$\frac{I_t}{I_i} = \left(1 - \frac{A}{1-R}\right)^2 \left(\frac{1}{1+F\sin^2\delta}\right) \qquad (4)$$

The reflection coefficient R in this case is equal to R = 1-T-A, where A denotes the absorbtion coefficient. Thus the intensity may become reduced considerably, and the reflection coefficient R used in Eq. 2 is altered. In the following parts of this section the expression for transmitted light intensity, given in Eq. 3, is used to derive theoretical values for use in the evaluation of the characteristics of the SFPI constructed.

B. Separation of the Modes

In the case of non-confocal spherical mirror resonators, [5] the field solutions of Maxwell's equations, satisfying the boundary conditions, have well defined spatial distributions of the electromagnetic fields, classified as TEM_{mnq} modes. [4,5,6] For best use of the SFPI, primary concern is with the TEM_{00q} mode, where the transverse field distribution is approximately Gaussian, as shown in Fig. 1.

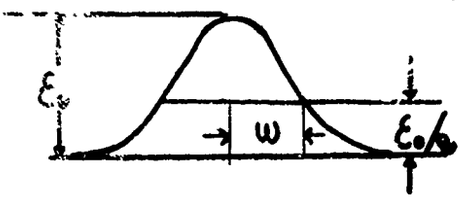

Fig. 1. Transverse field distribution of the fundamental TEM_{00q} mode.

For normal incidence, in air, the expression for wavelength as a function of mode numbers m, n, and q is written: [6]

$$\frac{2L}{\lambda} = q + \frac{1}{\pi}(1 + m + n)\cos^{-1}\left(1 - \frac{L}{R}\right) \qquad (6)$$

For the case where R≫L, and m =0, n=0, one obtains q = 2L, with q, the axial mode number, usually of the order of magnitude q= 10^4 to 10^6. With $\delta = \frac{2\pi L}{\lambda}$, resonance or maximum light transmission is achieved according to Eq. (3) and (6) when L is an integral number of half-wavelengths.

In terms of frequency it readily follows from Eq. (6) that:

$$\nu_0 = \frac{qc}{2L} \qquad (7)$$

This is the center frequency at which the maximum light transmission occurs in the interferometer. Separation in frequency between adjacent transmission maxima, or resonances, occurs in the cavity at:

$$\nu_{q+1} - \nu_q = \frac{c}{2L} \qquad (8)$$

This is a well known [18] expression for the interferometer free spectral range or mode frequency separation, which is identical to the expression for the laser free spectral range determined by the Fabry Perot etalon used as the laser resonator. From the above it is readily seen that the separation of the modes in the resonant cavity with a typical reflector spacing of L= 7.5 cm is 2.0 Gc/s. Fig. 2 [17] shows the variation of the relative transmitted light intensity $\frac{I_t}{I_i}$ vs. frequency ν as a function of the mirror reflectivity R. Also shown in Fig. 2 is an indication of the Fabry-Perot interferometer free spectral range $\frac{c}{2L}$.

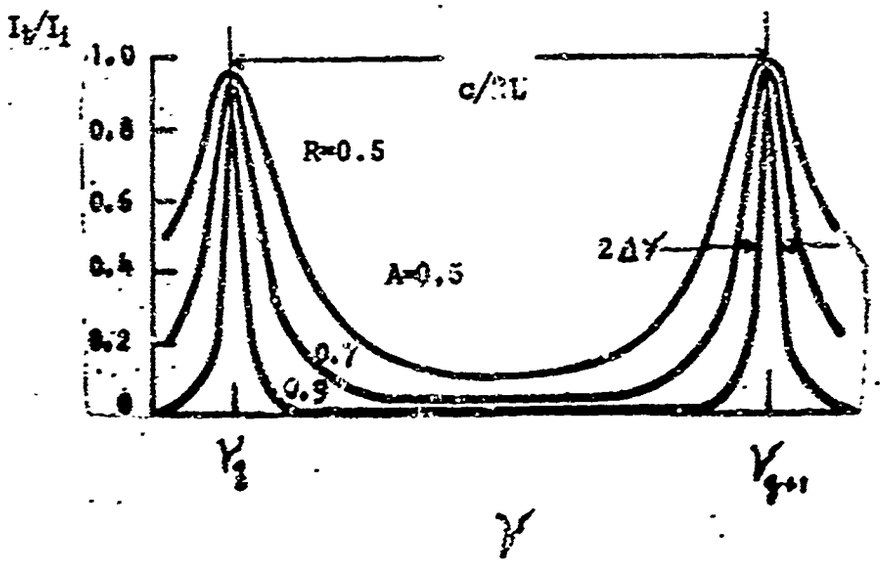

Fig. 2 The Fabry Perot interferometer light transmission characteristic I_t/I_i vs. frequency as a function of mirror reflectivity R. The absorbtion coefficient is A, the half-intensity width is $2\Delta\nu$, and the interferometer free spectral range is c/2L.

C. Half-Intensity width and minimum light transmission

The half-intensity width $2\Delta\nu$ which is shown in Fig. 2, is derived from Eq. (3) when $\Delta\delta = \frac{(1-R)}{2\sqrt{R}}$, i.e., for small δ. For a particular reflector separation L one obtains:

$$2\Delta\nu = \frac{1-R}{\pi\sqrt{R}} \left(\frac{c}{2L}\right) \tag{9}$$

The minima in transmitted light intensity occur whenever the distance L is an odd multiple of quarter wavelengths, i.e., when $\delta = (2n+1)\frac{\pi}{2}$; $(n=0,1,2 \ldots)$. The expression for these minima is written

$$\frac{I_{t(min)}}{I_i} = \frac{1}{1 + \frac{4R}{(1-R)^2}} = \frac{1}{1+F} \tag{10}$$

Calculation with R = 0.99 yields $I_t/I_i = 1.02 \times 10^{-4}$. This characteristic is important for the resolution of modes with weak amplitudes or modulation sidebands in the presence of unwanted noise or interference.

D. Finesse and Resolution

Fig. 3. shows a plot of adjacent resonances given by c/2L for the scanning Fabry Perot interferometer for various reflector separations L. Finesse $\mathcal{F}$ is defined [17] as the ratio of the separation of these resonances or peaks in light intensity transmission c/2L to the half-intensity width $2\Delta\nu$. The finesse $\mathcal{F}$ is thus found to be $\frac{\pi\sqrt{R}}{1-R}$. Fig. 4 shows the interferometer finesse $\mathcal{F}$ as a function of mirror reflectivity R. Hence a direct relation exists between finesse $\mathcal{F}$, reflector separation L, and mirror reflectivity R. Fig. 5. shows this relation in terms of half-intensity width $2\Delta\nu$ vs. interferometer mirror separation L_i as a

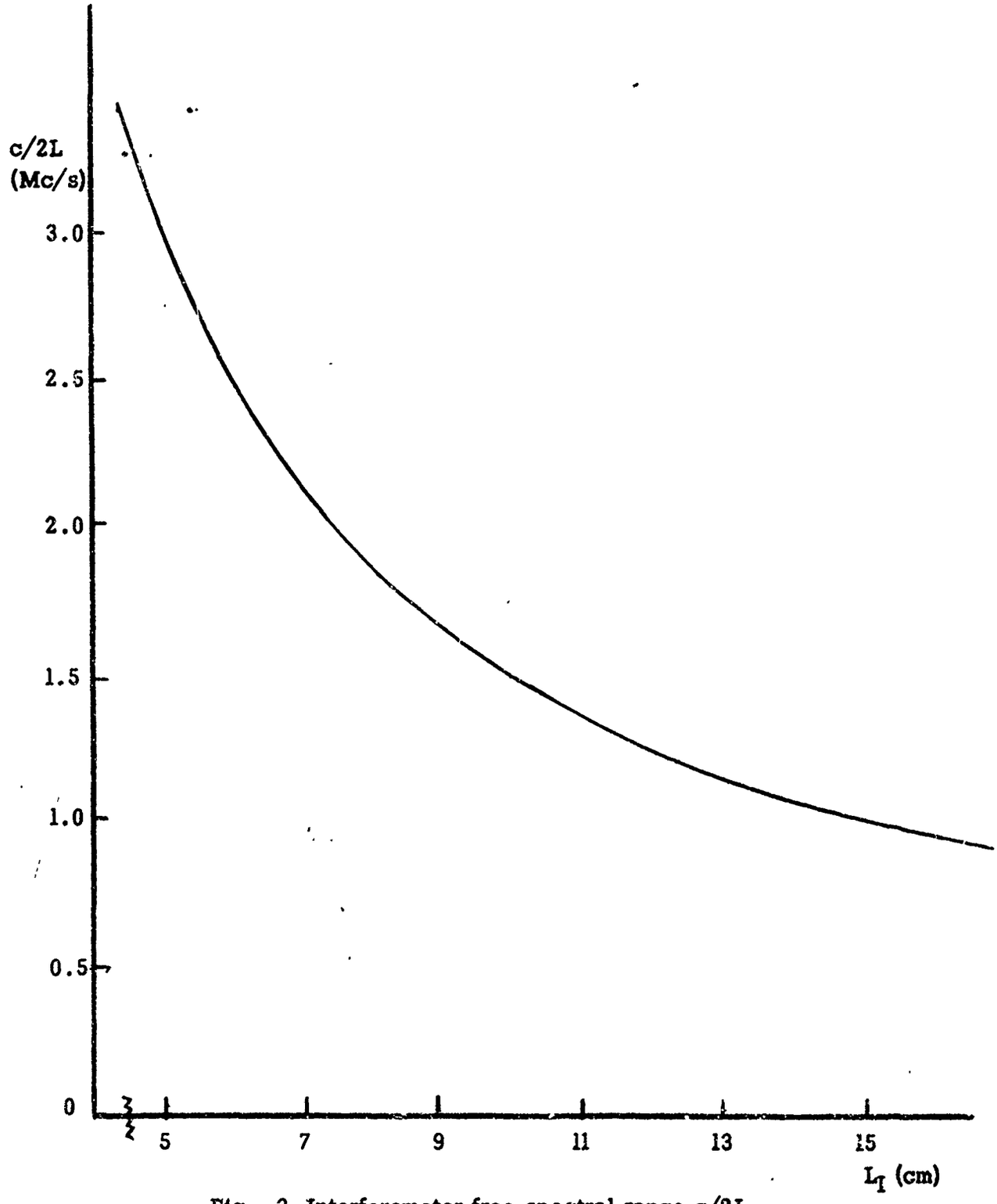

Fig. 3 Interferometer free spectral range c/2L vs. separation of the mirrors L_I.

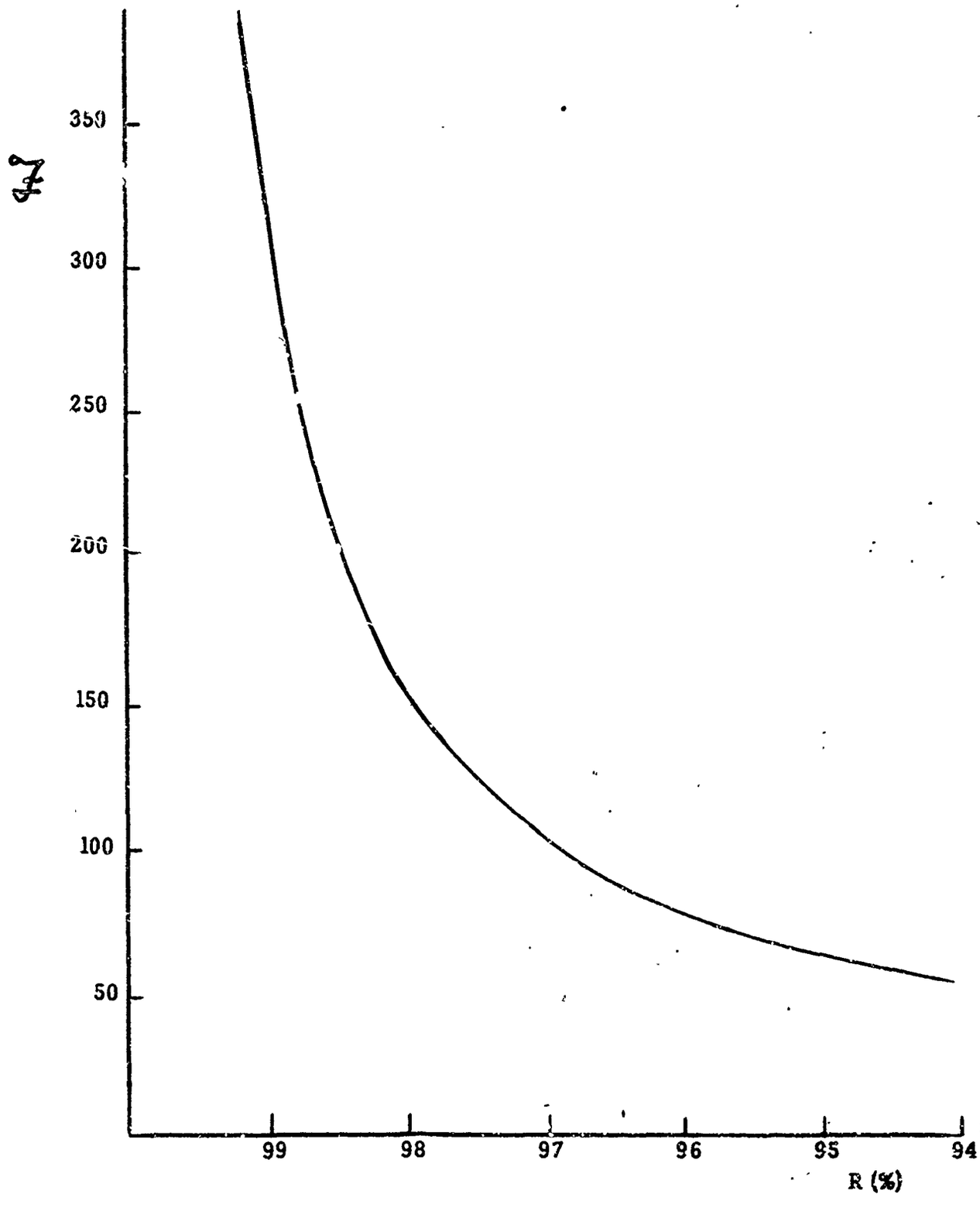

Fig. 4 Finesse $\mathcal{F}$ of the interferometer vs. reflectivity of the mirrors R%.

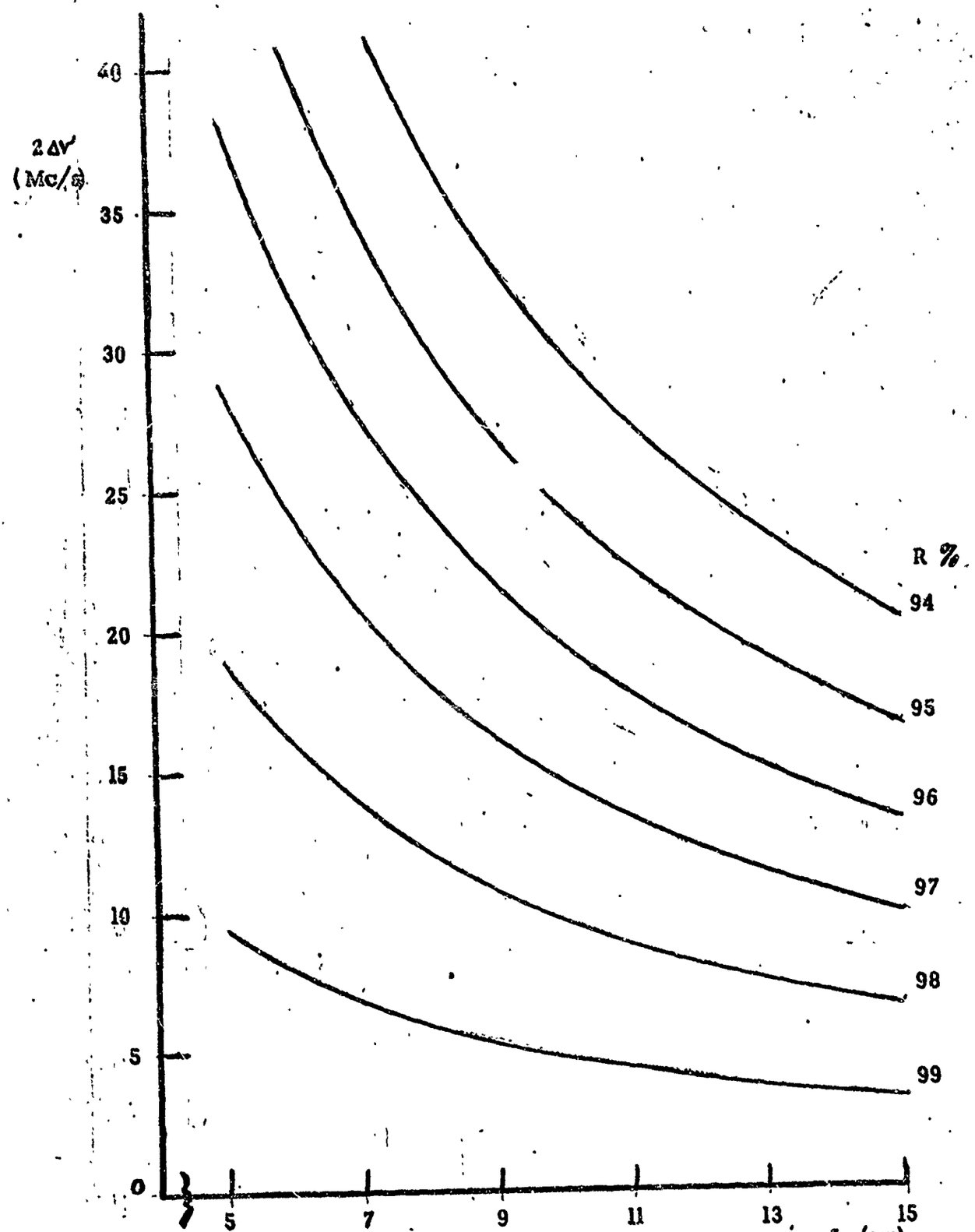

Fig. 5 Interferometer half-intensity width $2\Delta\nu'$ vs. interferometer mirror separation L_I as a function of mirror reflectivity R

function of mirror reflectivity R.

Values of half-intensity width $2\Delta\gamma$ and finesse $\mathcal{F}$ are particularly useful in the evaluation of the performance of the SFPI.

An important characteristic of the SFPI in it's high resolving power. This resolving power is:

$$\frac{\gamma_0}{\Delta\gamma} = \frac{2\mathcal{F}L}{\lambda} \tag{11}$$

The value of the resolving power $\frac{\gamma_0}{\Delta\gamma}$ is found to be equal to 7.34×10^7 for a reflector separation of 7.5 cm and a mirror reflectivity of 99%. This value is based on consideration of visual sensitivity [17] whereas actual resolution, when viewing an oscilliscope presentation of spectral information, is considerably higher. A relation exists between this resolving power, derived by classical optical theory, and its counterpart derived in quantum theory, as pointed out by Boyd and Gordon [5]. Considering the quality factor Q of an optical resonater with light waves reflected back and forth between the mirrors, one obtains:

$$Q = \frac{2\pi L}{\alpha\lambda} \tag{12}$$

Where α is the fractional power loss per reflection. The two expressions of Eqs. (11) and (12), for resolving power $\frac{\gamma_0}{\Delta\gamma}$ and quality factor Q respectively show the correspondence between classical and quantum mechanical formulas when α is approximated as 1-R, and it is recalled that in Eq. (11), $\mathcal{F} = \frac{\pi\sqrt{R}}{1-R}$.

E. Summary

In this section the basic theory of the scanning Fabry Perot interferometer light transmission characteristics is reviewed. Half-intensity width $2\Delta\nu$, finesse $\mathcal{F}$, and interferometer resolution are related to the physical parameters of the instrument, viz., mirror reflectivity R and mirror separation L. These characteristics will be used in Section 5 for evaluation of the output characteristics of the constructed SFPI.

3. Matching of the Modes

A. General matching requirements

Excitation of the fundamental TEM_{00q} mode in the SFPI cavity presents three major requirements:

(1) precise axial alignment of the SFPI with the laser beam;

(2) proper matching of the traveling-wave field of the laser radiation to the traveling waves established within the SFPI; and

(3) isolation of the laser resonator from the reflected energy from the SFPI .

These requirements are now discussed in some detail.

(1) It has been noted [19] that a misalignment of the SFPI with respect to the laser beam, caused by a tilt or an axial displacement of the interferometer mirrors, results in the excitation of higher order transverse modes within the SFPI cavity. This off-axis alignment causes a reduction in the interferometer finesse $\mathcal{F}$. In addition, the presence

of unwanted off-axis modes causes distortion and interference in the SFPI fundamental modes or modulation sidebands, when present.

(2) The second condition for successful utilization of the SFPI is proper mode matching or coupling to the laser radiation. [20]. Efficient coupling of the coherent laser light modes into the SFPI cavity requires the matching of the diameter and phase front curvature of the incoming laser beam to the corresponding characteristics of the fundamental interferometer mode. Consideration of the pertinent matching parameters, viz., beam radius w, minimum beam radius w_0 and minimum beam radius position $\bar{z}_0$, is described in Section 3 B. Section 3 C summarizes the general matching procedures for typical laboratory configurations. Section 3 D presents useful matching graphs for the SFPI constructed. It is suggested that for other SFPI configurations a similar set of graphs be prepared as they greatly simplify the application and matching of the SFPI to the laser output.

(3) In addition to the above requirements for proper coupling of the laser radiation into the fields existing in the SFPI, there remains the need for isolation of the laser from the energy reflected from the SFPI which can couple with oscillating laser modes. Isolation is achieved through the use of a linear polariser and a quarter-wave plate positioned in the laser beam as near the laser as practicable. This arrangement is shown in Fig. 6 with the polariser being closest to the laser. The polarizer is aligned with the laser polarization and the quarter-wave plate optic axis is oriented 45° with respect to the axis of laser light polarization. Upon passing through the isolation combination

the light becomes circularly polarized. When reflected from the SFPI receiving mirror, the direction of rotation is reversed for the circularly polarized light, and upon passing back through the quarter-wave plate, this reflected light polarization is now orthogonal to the polariser axis and it is thus attenuated. [18]

B. The Matching Parameters

The required parameters [6,21] for proper mode matching between the laser and the SFPI are

(1) beam radius w, also called the spot size of half-width for the fundamental TEM_{00q} mode. This parameter is shown in Fig. 1 as the radius of the circle of the transverse amplitude distribution where the amplitude E_o has decreased to the value E_o/e.

(2) minimum beam radius w_0

(3) location of the minimum beam radius z_0 This is the axial distance from the mirror to the internal position of the minimum beam radius w_0.

For a resonator with a pair of spherical reflectors with radius of curvature R_c and separation L, the beam radius at a reflector is written: [6]

$$\omega_{L(z)} = \sqrt{\frac{\lambda}{\pi}\frac{2}{}} \left(\frac{2R_c}{L} - 1\right)^{-\frac{1}{4}} \qquad (13)$$

The minimum beam radius is: [6,15]

$$w_{1(2)}^{2} = w_{L(2)}^{1}\left[\frac{\left(\frac{2R_c}{L}\right)-1}{\left(\frac{2R_c}{L}\right)-1+\mu^2}\right] \tag{14}$$

The apparant[2] location of the beam minimum is: [6,15]

$$Z_{L(2)} = \frac{\mu R_c}{2\left(\frac{R_c}{L}\right)-1+\mu^2} \tag{15}$$

In eqs. (13), (14), and (15) the subscripts L and I denote laser and interferometer respectively as do the subscripts 1 and 2.

The minimum beam radii w_1 and w_2 and their locations Z_L and Z_I are of particular importance in the proper matching of the SFPI to the transmitted laser light. Kogelnik [20] has analysed the matching problem from which two basic formulas, Eqs (16) and (17), ensued. Kogelnik determined that the laser beam is properly transformed or coupled into the natural mode of the SFPI by the focussing effect of a lens or lens system inserted in the beam at distances d_1 and d_2 from the respective locations of w_1 and w_2. The distances d_1 and d_2 are:

$$d_1 = f\left[1 \pm \frac{w_1}{w_2}\sqrt{1-\left(\frac{f_0}{f}\right)^2}\right] \tag{16a}$$

$$d_2 = f\left[1 \pm \frac{w_2}{w_1}\sqrt{1-\left(\frac{f_0}{f}\right)^2}\right] \tag{16b}$$

Where f is the focal length of the matching lens and f_0 is a characteristic length given by:

$$f_0 = \frac{\pi}{\lambda} w_1 w_2 \tag{17}$$

[2]The appearance of μ index of refraction, in Eqs. 14 and 15, accounts for a diffraction effect caused by the geometry of the reflector, where the external surface of the spherical mirror is flat. Further discussion of this effect is given in Ref. (15).

In Eqs. (16a) and (16b) f must be greater than f_0 and the same sign must be chosen.

C. Summary of the matching procedures

Three matching procedures are summarized below in terms of the parameters presented in Section 3 B. Case I is the general case and Cases II and III are special cases derived from Case I. These procedures were successfully applied for each of the cases described. The procedures involve essentially a set of calculations which determine the proper location of the SFPI and the matching lens with respect to the laser position.

Case I Spherical resonator. In this case the laser reflectors are both spherical with radius of curvature R_c and separation L_L.

(1) Determine w_L using a variable round iris and a power meter as follows:
Insert the iris in the laser beam at the transmitting mirror. Decrease the iris diameter (2w) until the meter power reading is reduced by 13.5 per cent from the full aperture reading. The iris diameter at this point is $2w_L$.

For this case w_L may also be calculated from Eq. (13).

(2) From Eq. (14) calculate w_1.

(3) From Eqs. (13) and (14) calculate w_I and w_2 using the appropriate R_c and L_I for the interferometer.

(4) From Eq. (15) calculate Z_L and Z_I, again using the appropriate R_c and L for the respective laser and interferometer calculations.

(5) From Eq. (17) calculate f_0.

(6) Select a lens of focal length $f > f_0$, and calculate the distances d_1 and d_2 according to Eqs. (16a and b).

(7) From d_1 and d_2, Z_L and Z_I determine the location of the SFPI and the position of the matching lens according to Fig. 6a. The SFPI will thus be a distance $d_1+d_2-Z_L-Z_I$ from the laser.

Case II Hemispherical resonator, collimated. In this case one of the spherical mirrors is replaced by a flat mirror and the laser beam is transmitted from the spherical mirror through built-in collimating optics.

(1) Determine w_L using the variable round iris as in Case I.[3]

(2) For the collimated beam $w_1=w_L$ and $Z_L = 0$.

(3) Determine w_2, f_0, and Z_I as in Case I.

(4) Select a lens with $f = f_0$ or use a pair of thin lenses to achieve a combined $f = f_0$ according to:[4]

$$\frac{1}{f} = \frac{1}{f_1} + \frac{1}{f_2} - \frac{\ell}{f_1 f_2} \qquad (18)$$

where f_1 and f_2 are the thin lens focal lengths, and ℓ is the required separation.

(5) The matching lens (or pair of lenses) is positioned at the laser and the location of the SFPI is determined at a distance f_0-Z_I, according to Fig. 6b.

[3]For the hemispherical resonator w_L may be calculated from the following Eqs.:

$$w_L \text{ (spherical mirror)} = \left[\left(\frac{\lambda}{\pi}\right)^2 \frac{R_c^2 L}{R_c - L} \right]^{1/4} \qquad (19)$$

$$w_L \text{ (flat mirror)} = \left[\left(\frac{\lambda}{\pi}\right)^2 L(R_c - L) \right]^{1/4} \qquad (20)$$

The iris method above is recommended, however, since the accuracy attained is quite satisfactory for requirements.

[4]When using the double lens system to achieve the desired focal length $f=f_0$, adjustment of lens separation ℓ for best focus of w_2 is facilitated by holding a card inside the SFPI and slightly adjusting the lens closest to the laser until best focus of the beam on the card is obtained, as indicated by minimum spot size.

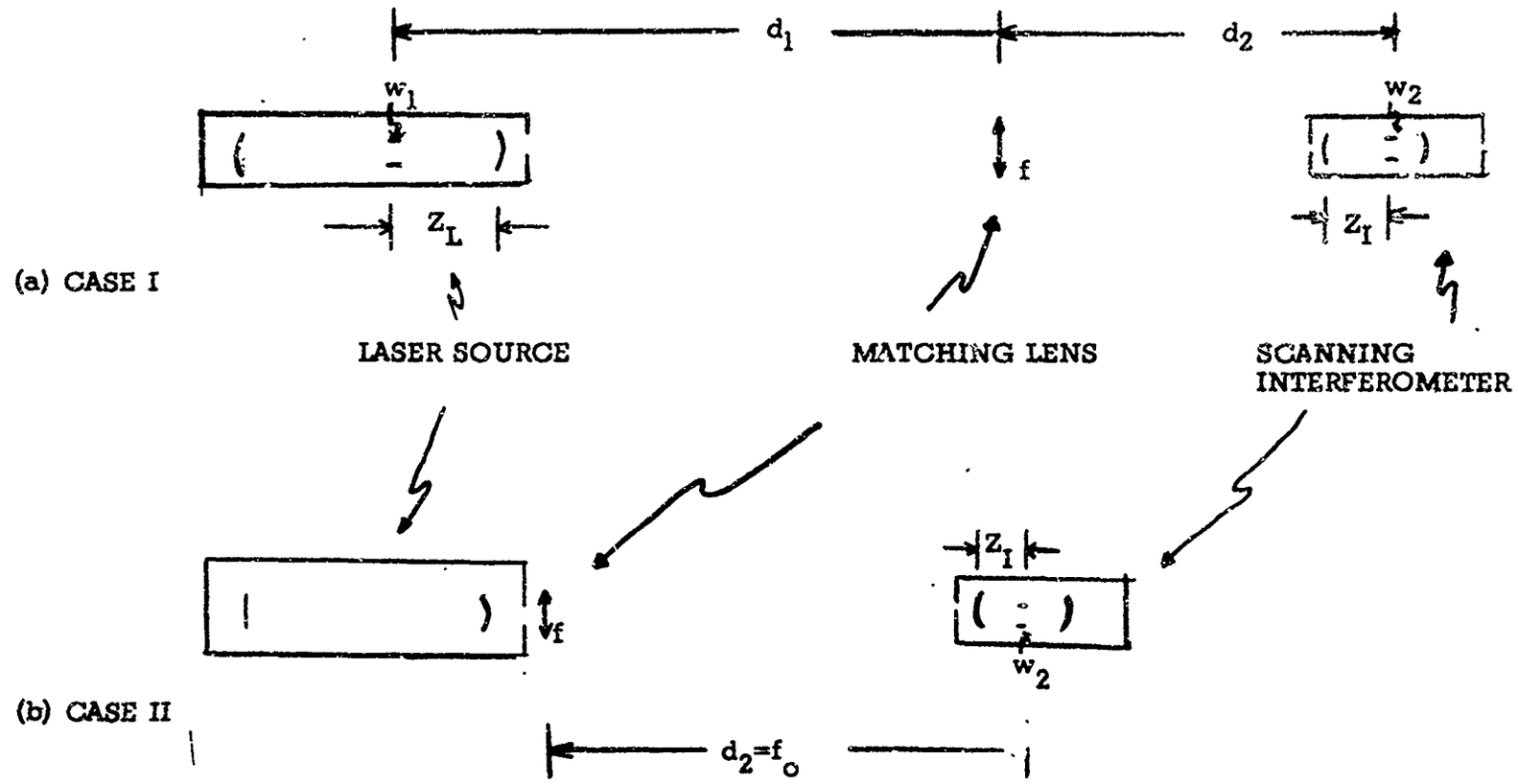

Fig. 6 Matching diagrams (a) Case I spherical resonator
(b) Case II hemispherical resonator

Case III Hemispherical resonator, uncollimated. In this case the laser mirrors are the same as in Case II but the laser beam emerges from the flat mirror and is uncollimated.

(1) Select an appropriate lens with a facal length f_c and collimate the laser output by placing this lens at a distance f_c from the transmitting mirror. Then the procedure is the same as in Case II for the collimated beam.

D. Specific matching graphs for the interferometer

Once a particular configuration is chosen for a SFPI construction, the matching procedures outlined above are considerably simplified by graphical methods. Graphs of the required parameters w_2, Z_I and f_0 may be prepared in advance for repeated use in all matching situations. The graphs presented in this section in Figs. 7, 8 and 9 are prepared for the SFPI evaluated, where the reflectors were spherical with radii of curvature R_c=3m, and their separation was variable over a range from 5 to 11 cm which was considered appropriate for prevention of ambiguity in the transmitted spectrum[5].

Fig. 7 shows values of the characteristic length parameter f_0 for various SFPI mirror separations L_I as a function of laser minimum beam radii w_1.

Fig. 8 shows variation of the parameter Z_I as a function of the interferometer mirror separation L_I.

Fig. 9 shows variation of the parameters w_2 and w_I as a function of interferometer mirror separation L_I.

[5]Further discussion of ambiguity problems is given in Section 4 E. For $L_I > 10$cm the interferometer free spectral range $c/2L$ is less than the Doppler broadened line and spectral displays show overlapping mode patterns.

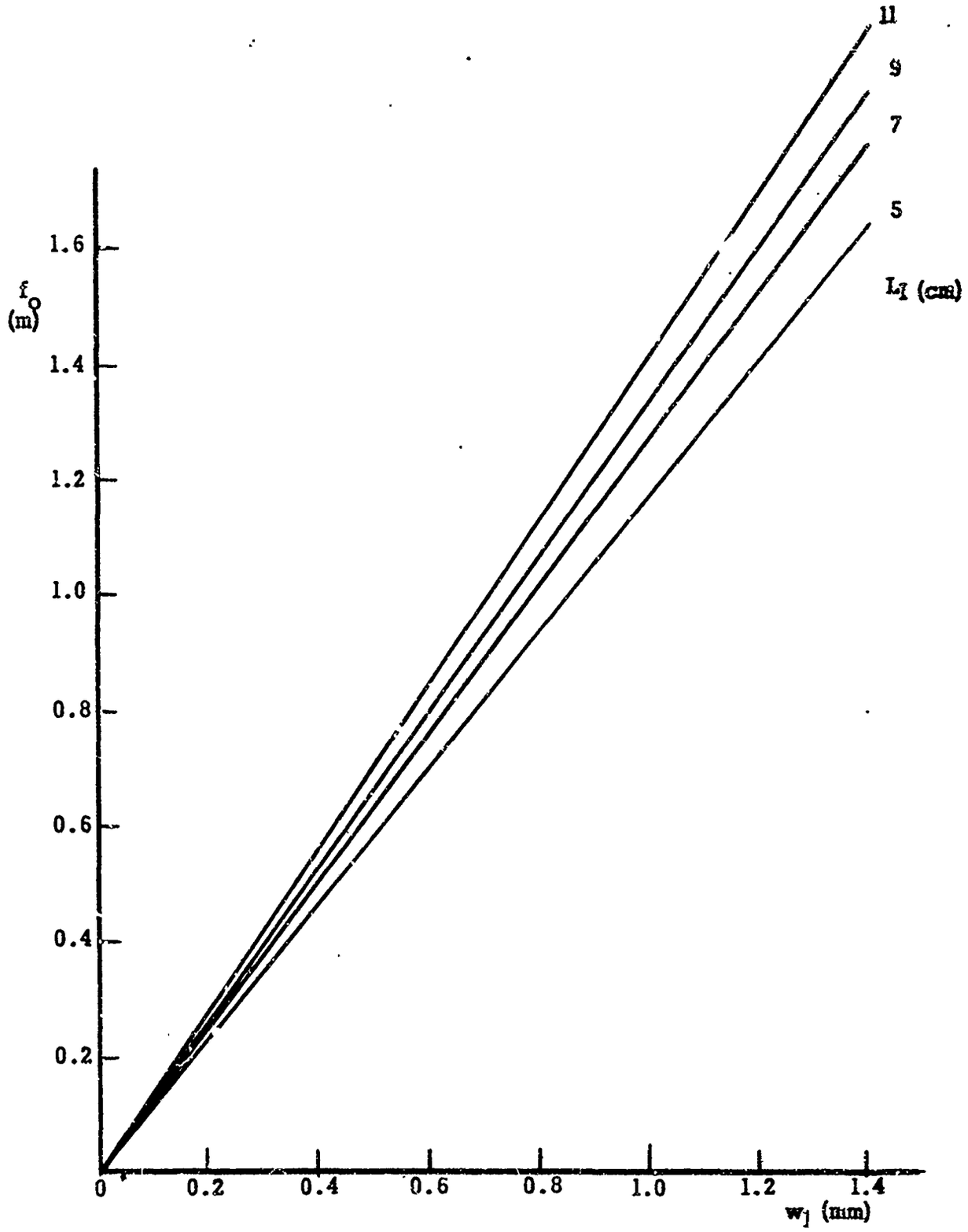

Fig. 7 Characteristic matching length f_o vs. laser minimum beam radius w_1 as a function of interferometer mirror spacing L_I .

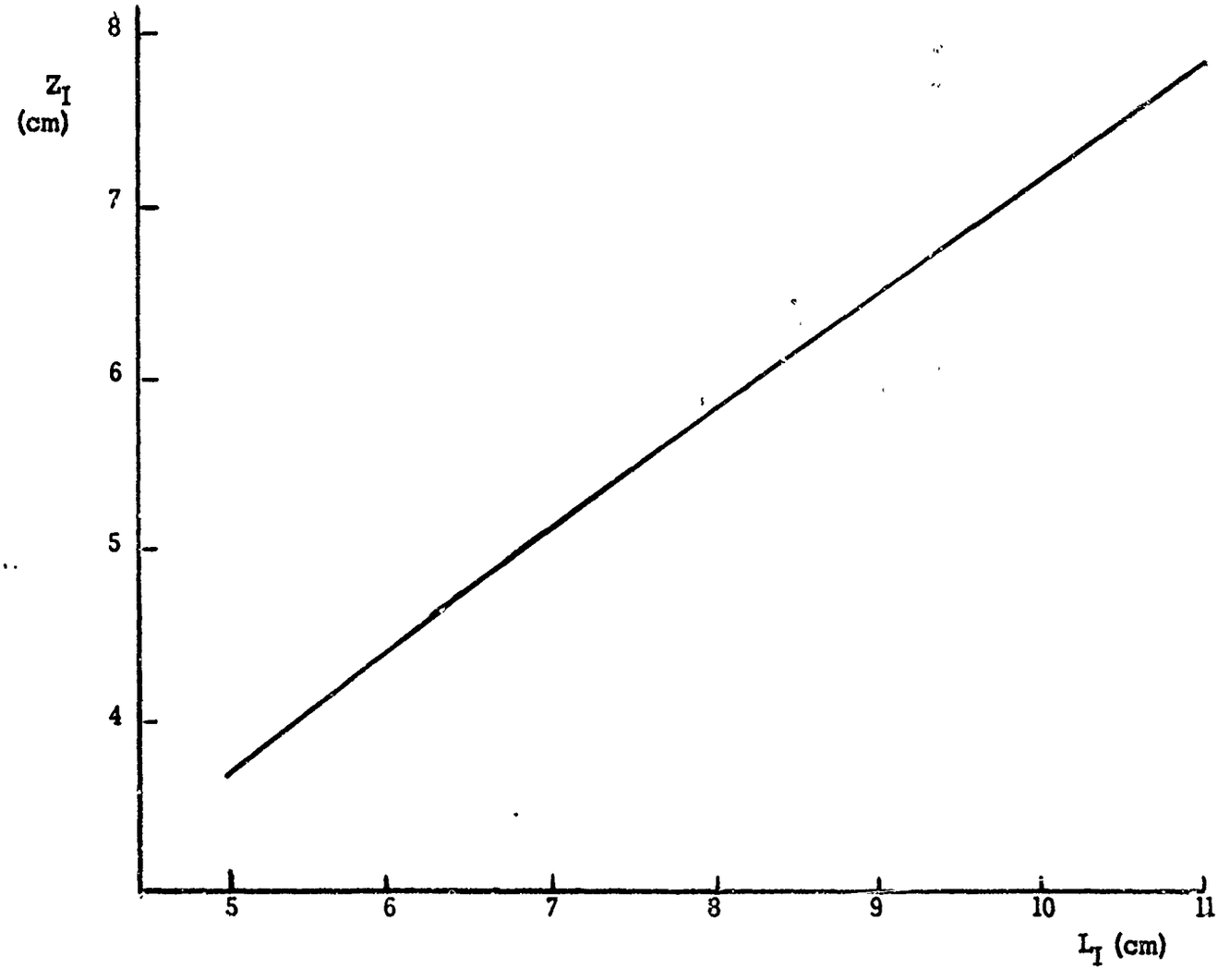

Fig. 8 Apparant location of the interferometer beam minimum Z_I vs. interferometer mirror separation L_I

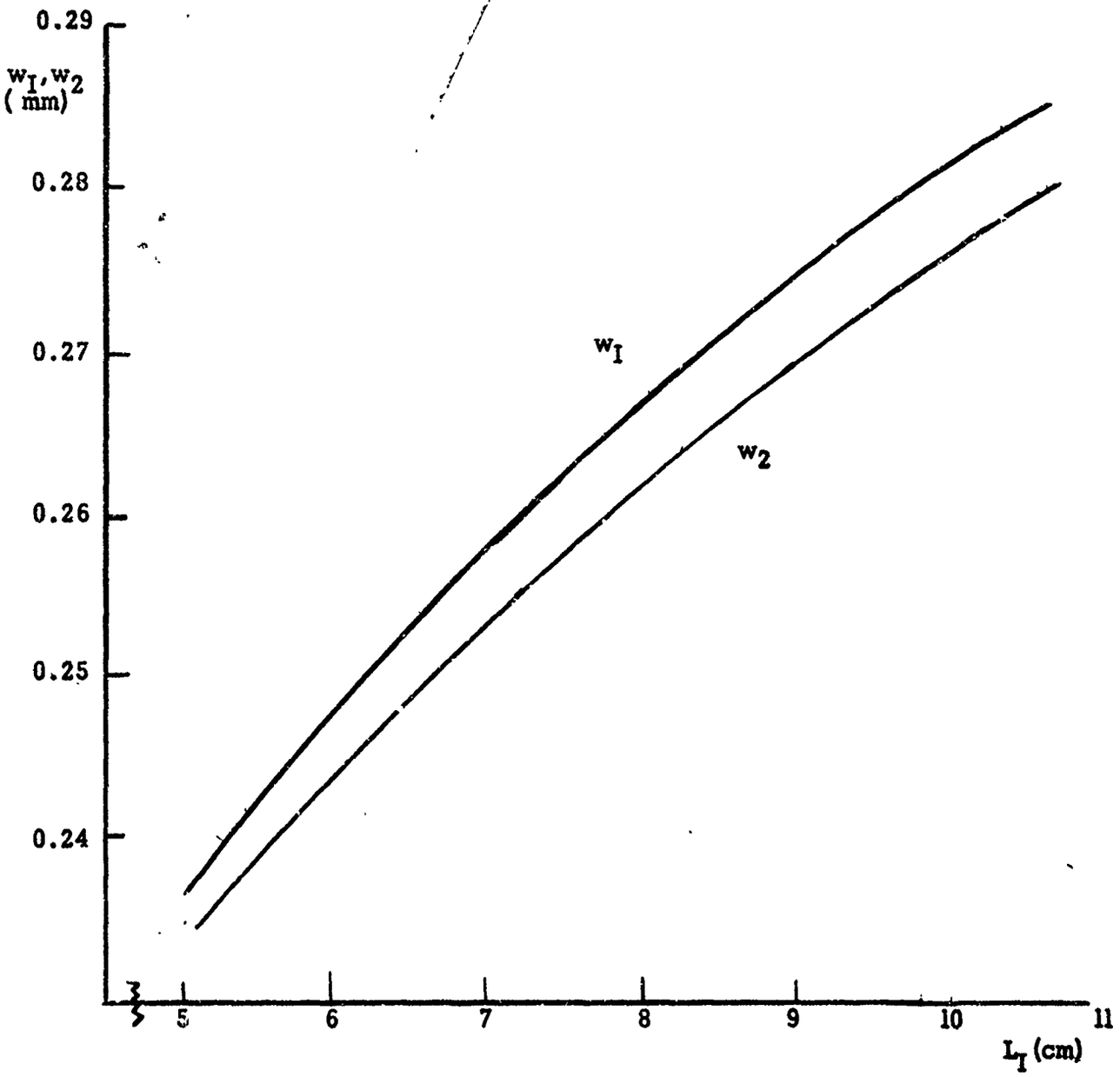

Fig. 9 Interferometer beam radii w_I and w_2 vs. mirror separation L_I.

E. Matching graphs for the Spectra Physics Model 116 laser

Additional graphs of the laser parameters Z_L, w_L and w_1 (defined on p. 13,14) may also be prepared for matching requirements for conditions where the laser reflector separation L_L may vary, as in the case of the Spectra Physics model 116 laser[6] used in the FM laser experiments described in Section 7. Graphs of the parameters Z_L, w_L, and w_1 are shown in Figs. 10, 11, and 12 respectively, for variation of laser mirror separation L_L from 100 to 200 cm. The laser mirrors were both spherical with radii of curvature R_c = 3 m.

Thus all the required matching parameters may be determined graphically, for rapid use in the matching procedures described in Section 3 C. A quick check of the laser minimum beam radius, w_1, (based on w_L) is recommended as a precaution, in the event there may be some additional effects such an internal modulator or aperture in the laser beam which may cause a variation of this parameter.

[6]Spectra Physics Corp. Mountain View, California Preliminary Information Sheet Jan 1965 ,

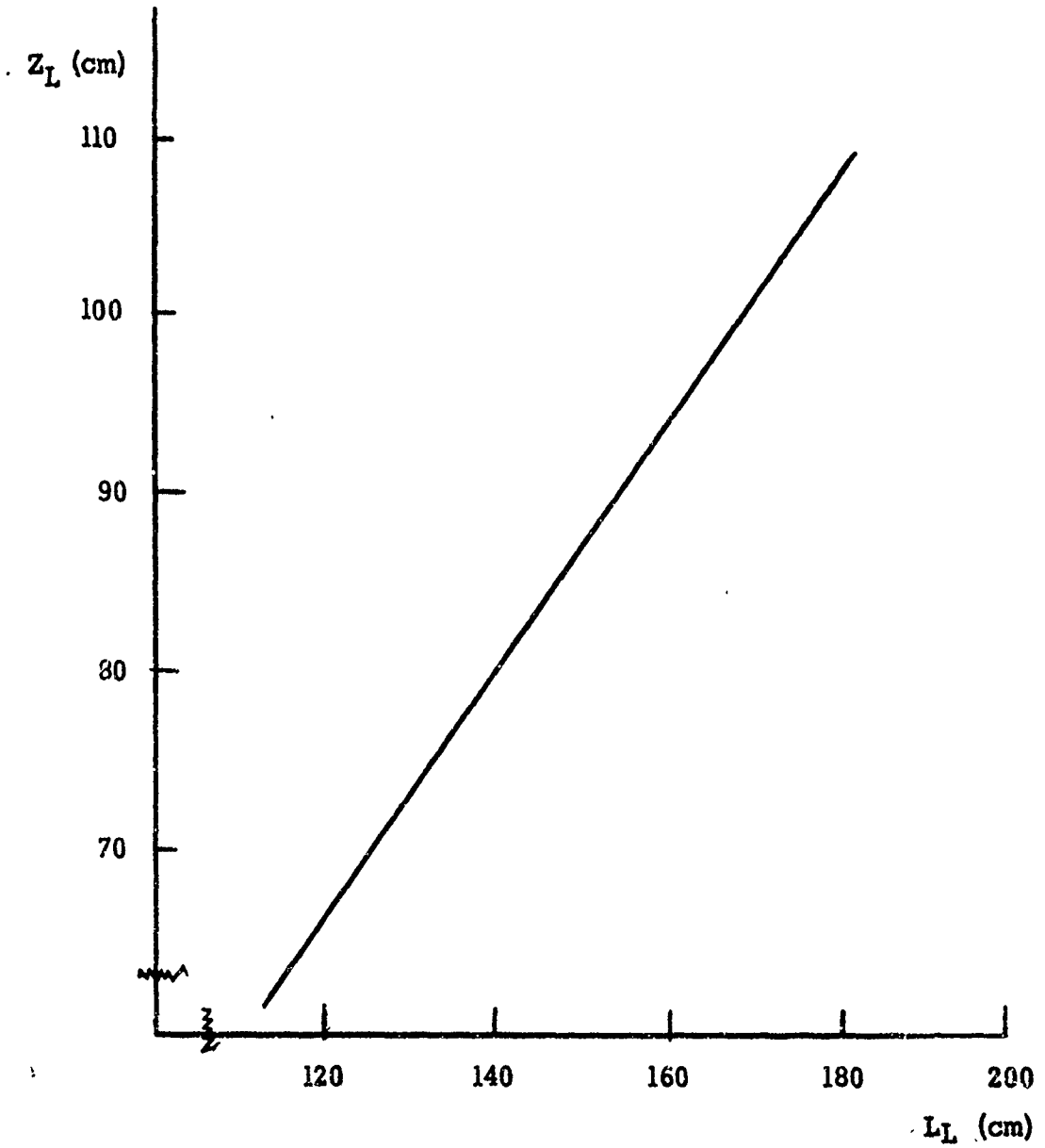

Fig. 10 Apparant location of the laser beam minimum Z_L vs. laser mirror separation L_L.

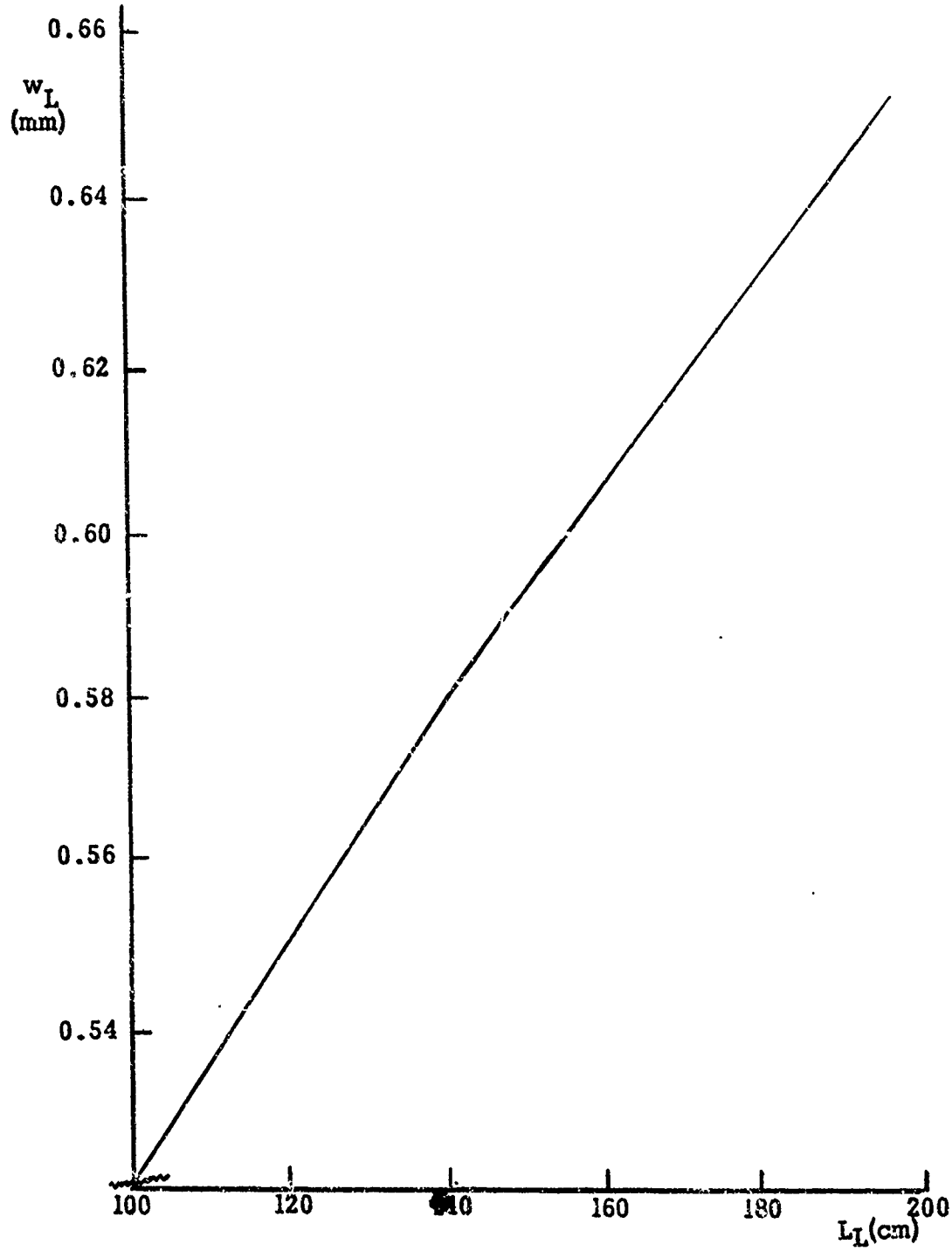

Fig. 11 Laser beam radius w_L at a mirror vs. mirror spacing L_L.

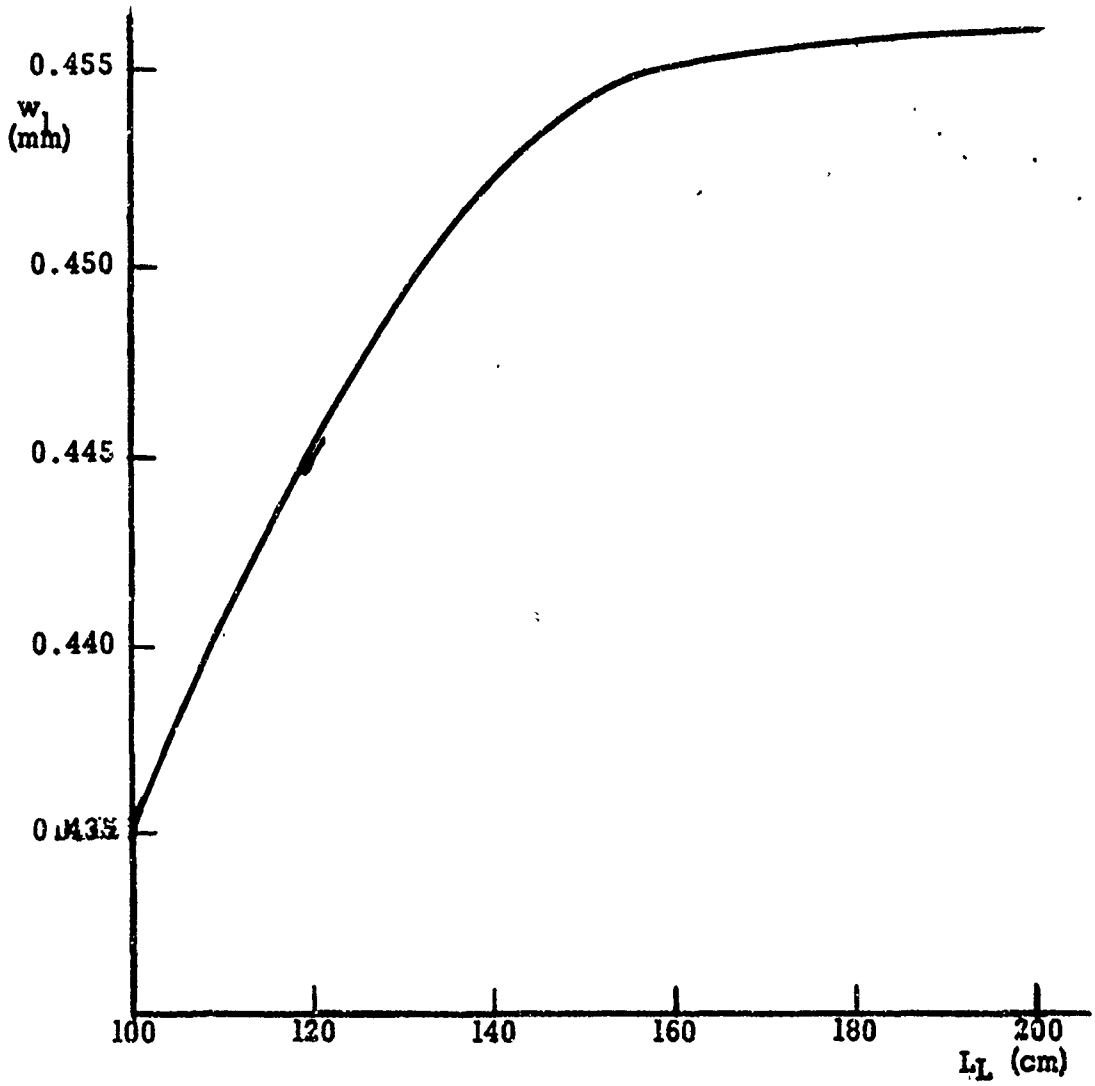

Fig. 12 Laser minimum beam radius w_1 vs. mirror spacing L_L.

4. Construction and operation of the interferometer

A. Description of the apparatus

The main structure of the SFPI is shown in Fig. 13. The SFPI consists of two vertical plates of aluminum ground stock which are fixed to a horizontal plate about one meter in length. The two vertical plates support four invar spacer rods. One end of the horizontal plate is hinged with spring steel to a main base plate and the other end can be moved with vertical and lateral freedom for the purposes of alignment of the SFPI. This motion is provided for by the two vernier controls (B) which are shown in Fig. 13. Fig. 14 shows the mounting of the SFPI front receiving mirror.(A) This mirror is cemented to a hollow ceramic piezoelectric transducer (B) which is in turn mounted in an aperture in the front face plate. The piezoelectric transducer provides axial motion of the receiving mirror and thereby scans the SFPI resonance across the portion of the spectrum which contains the laser modes. This transducer and mirror scan is described in detail in Part C of this section.

The rear mirror mounting assembly is shown in Fig. 14. A third vertical plate which carries the rear mirror mounting assembly, is supported and axially guided by the four invar spacer rods. The location of this vertical plate and thus the rear mirror, determines the basic SFPI reflector spacing L_I, and thus the interferometer free spectral range. The rear mirror (C) is located in a retaining holder which is in turn placed in an aperture in a circular mounting disc (D), as shown in Fig. 14. These controls provide a tilt of the circular mounting disc about axes that are oriented 60 degrees from the vertical to avoid confusion with

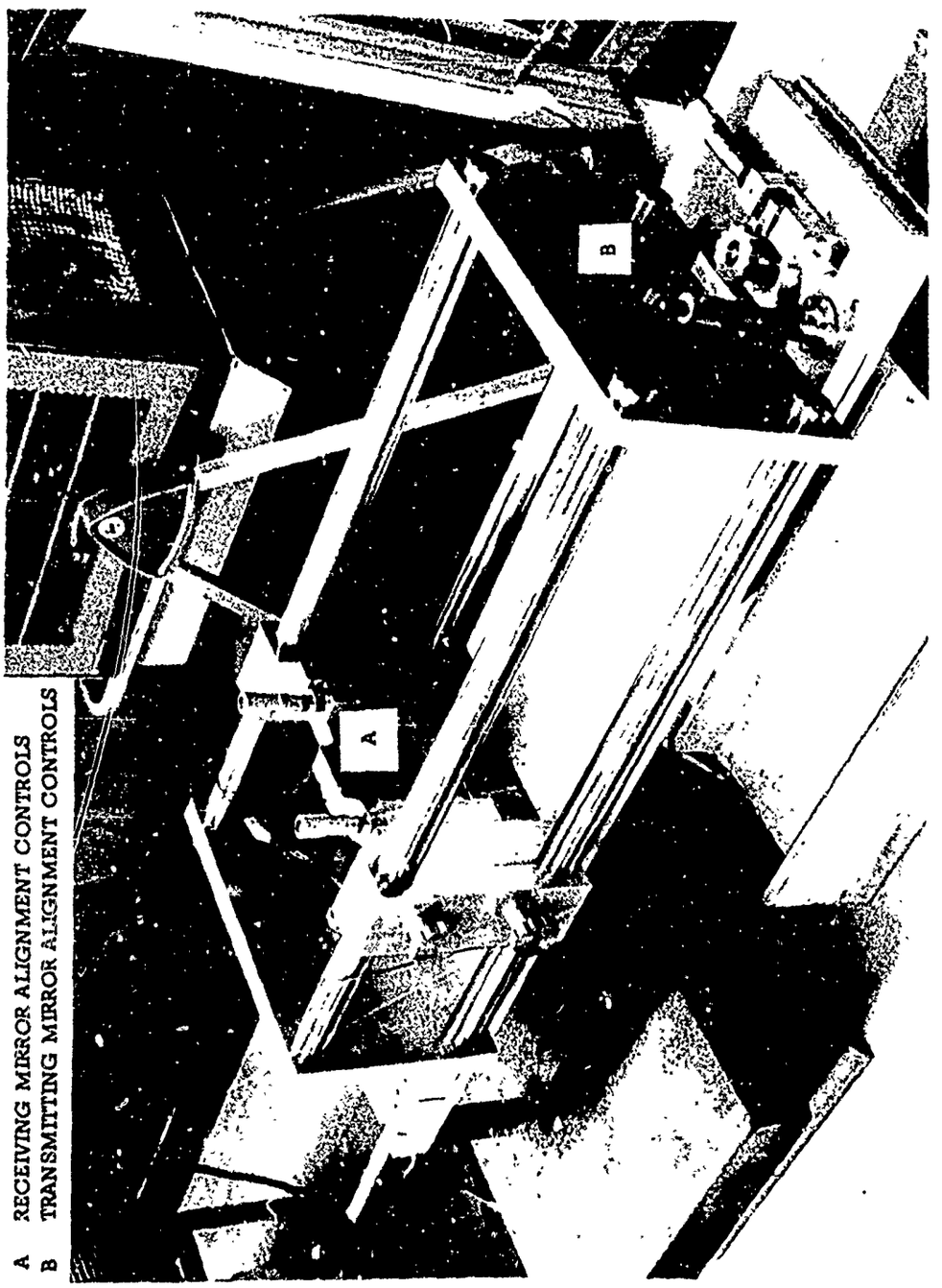

Fig. 13 Overall view of the scanning Fabry Perot interferometer showing alignment controls.

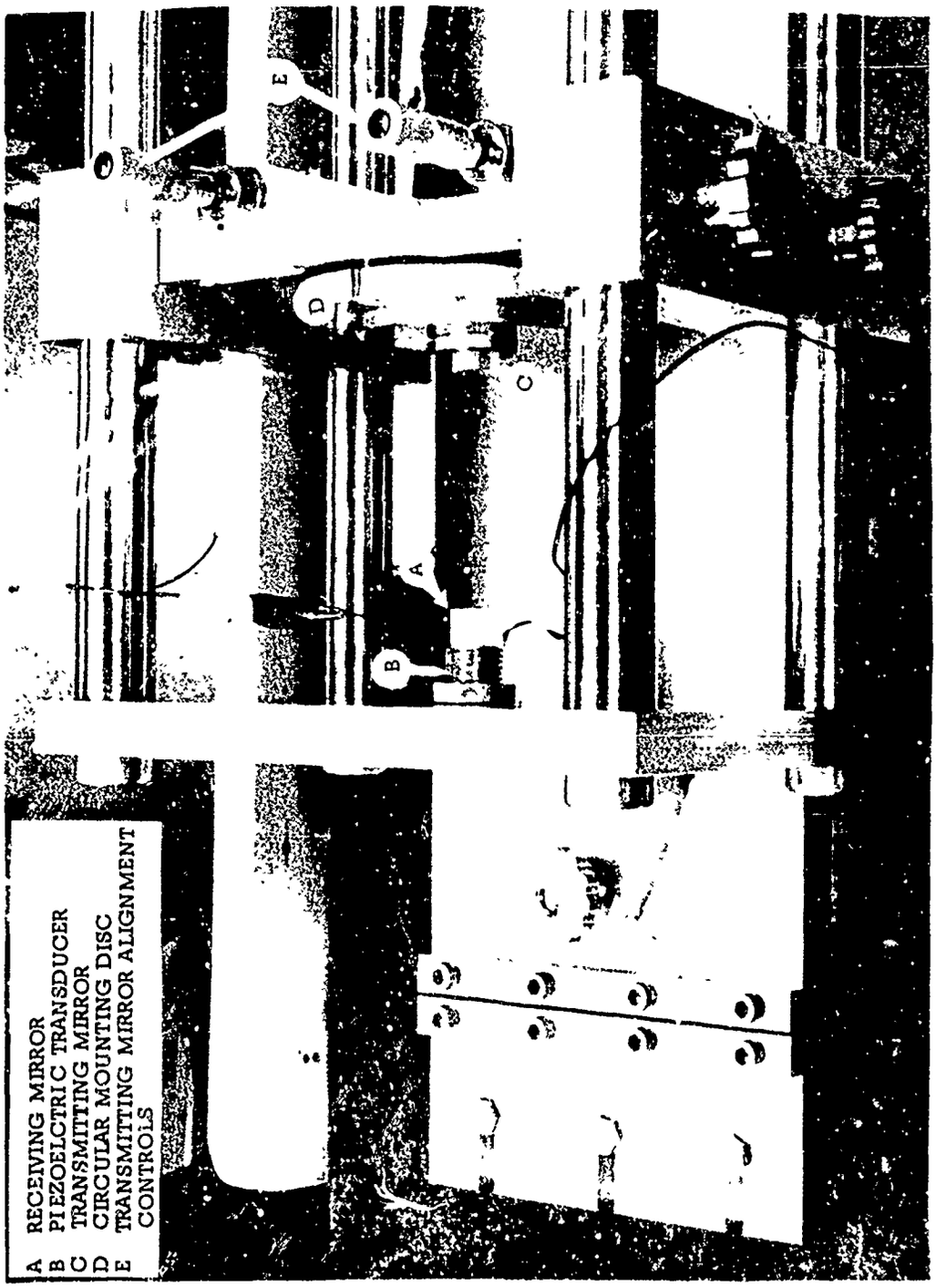

Fig. 14 Detailed view of the interferometer cavity showing the mirror mountings.

the vertical and horizontal control of the front mirror alignment. The circular mouting disc is attached to the vertical plate by beryllium springs which provide for positive control and avoid backlash effects.

The main base plate is supported at three points with provision for limited overall height variation during initial location of the SFPI with respect to the incoming laser beam. A suggested basic alignment procedure is described in part B of this section. The entire assembly was covered by a large plexiglass enclosure to prevent environmental disturbances such as drafts and airborne accoustic effects

The design of the SFPI constructed follows a pattern of one constructed at Bell Labratories [15] with variations in mirror mounting, alignment control and the use piezoelectric scan drive vice the moving coil system for improvement and experimental requirements.

B. A preliminary alignment procedure

The initial physical alignment of the SFPI with the laser beam is achieved through adjustment of the position and alignment controls described in the previous part of this section as follows:

After determining the position of the SFPI with respect to the laser, according to the matching procedures described in Section 3 C, the structure is placed so that the incoming laser beam passes through the front face plate aperture and the front mirror mounting assembly. The front mirror alignment is then adjusted (by means of vernier controls B, Fig. 13) until coaxial alignment of the laser beam and the SFPI cavity is achieved. This may be determined by placing a suitable small aperture in

the laser beam and adjusting the alignment, until the reflection of the laser beam from the receiving mirror (A, Fig. 14.) passes back upon itself, i.e., through the small aperture from which it originally came. Finally, the rear, transmitting mirror alignment is adjusted (by means of controls E, Fig. 14.) until the far field pattern of the SFPI output beam becomes a single, well defined bright spot with the TEM_{00q} mode amplitude distribution. Slight readjustment of the receiving mirror controls (A) Fig. 13 may be required. Magnification of the far field pattern may be obtained as necessary by placing a diverging lens at a practicable position in the output beam of the SFPI.

This completes the initial alignment procedure. After a discussion of the piezoelectric scanning technique and the method of detection and presentation of the SFPI output, the final method for precise alignment of the SFPI will be discussed.

C. Piezoelectric scan and display of the interferometer output.

This section describes the scanning technique, by which the passive SFPI resonance is swept over the laser output frequency spectrum, and a highly resolved presentation of the lasers spectral characteristics is obtained for visual study and analysis.

A piezoelectric ceramic transducer of lead titanate zirconate (henceforth abbreviated PZT-4) [22] was used (B, Fig. 14) to provide axial motion of the SFPI front mirror (A, Fig. 14), over a range greater than four half-wavelengths for $\lambda_o = 6328$ Å°. Manufacturer's specification for strain per applied voltage is approximately 8.8 Å° per volt,

(a) PZT- 4 TRANSDUCER

$d_{31} = -111 \times 10^{-12}$ meters/volt

$d_{33} = 256 \times 10^{-12}$ meters/volt

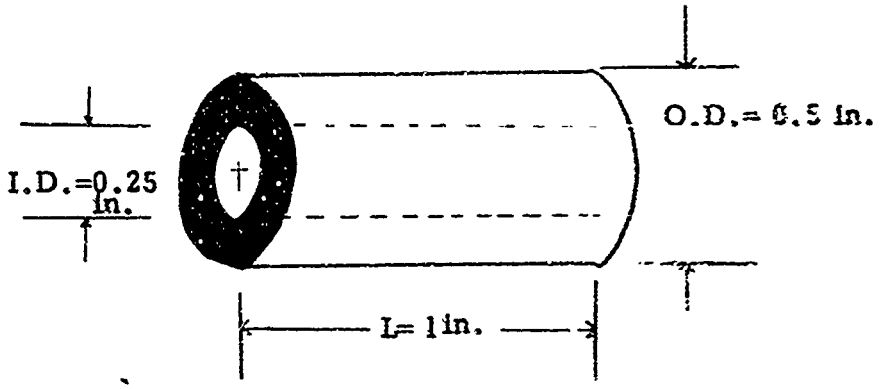

(b) PZT- 5 TRANSDUCER

$d_{31} = -140 \times 10^{-12}$ meters/volt

$d_{33} = 320 \times 10^{-12}$ meters/volt

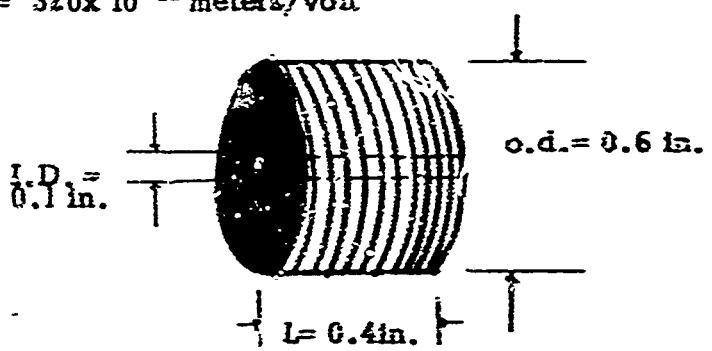

Fig. 15 The piezoelectric transducers
(a) The PZT-4 cylindrical tube configuration
(b) The PZT-5 stacked disc configuration

using a cylindrical PZT-4 tube with dimensions and strain constants as shown in Fig. 15a. Controlled transducer driving voltages up to the breakdown limit for the tube (1290 volts) were obtained from the combination of a variac and a 60 cycle line voltage transformer.

When using the PZT-4 transducer, with the variac control, driving voltage is simultaneously applied to the transducer and to the external sweep circuitry of a Tektronix 531 oscilliscope. This voltage caused the transducer to move the front mirror and thus sweeps the resonance of the SFPI across a limited portion of the optical spectrum which contains the oscillations or modes of the laser radiation. The light transmitted by the SFPI is received by an RCA 7102 photomultiplier, whose output is then applied for vertical deflection of the oscilliscope. Because of the sinusoidal nature of the driving voltage and thus the mirror motion proper blanking of the return sweep is required to eliminate a double trace presentation on the oscilliscope.

When the horizontal deflection of the oscilliscope is synchronized with the transducer driving voltage and thus the mirror scan, a linearly calibrated display of the optical power spectral density of the laser radiation including the number, intensity and relative position of the modes is presented on the oscilliscope.

For studies of the FM laser it was necessary to replace the PZT-4 transducer by a PZT-5 variety which is more sensitive. The configuration of the PZT-5 transducer and its strain constants are shown in Fig. 15b. This new transducer provides a scan of greater than onehalf wavelength at

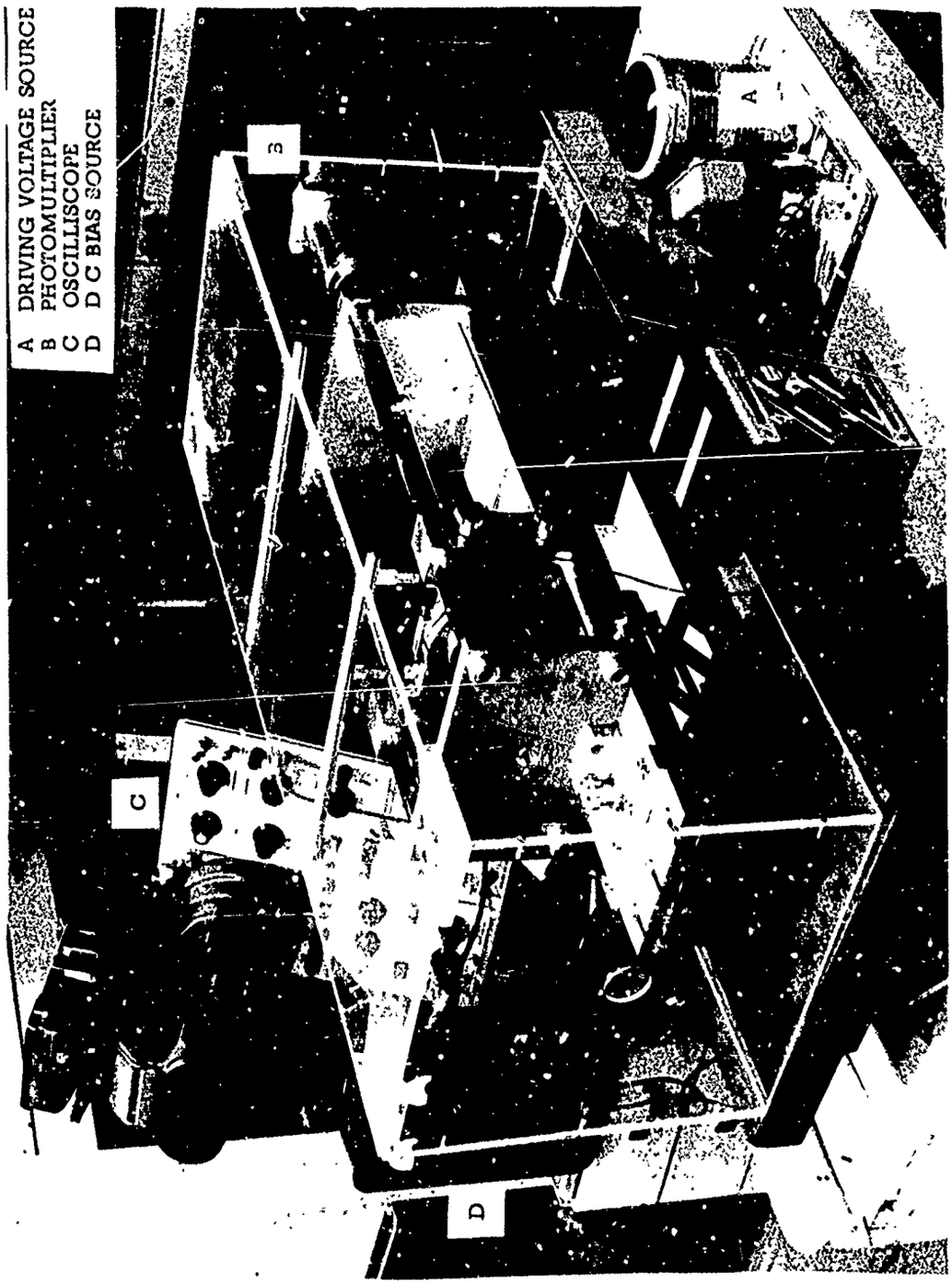

Fig. 16 A typical arrangement of required apparatus for laser spectral analysis with the interferometer enclosed in the plexiglass cover.

6328 A° when driven by a 150 volt sawtooth voltage from the oscilliscope deflection circuit. This sawtooth voltage was triggered externally so that synchronous presentation of the laser output was available when pulse modulation was applied.[7] Fig. 16 shows a typical arrangement of the SFPI and the required instruments for spectral analysis, including the driving voltage source (A), the photomultiplier (B), the oscilliscope (C) and a DC bias for the driving voltage (D).

D. Final alignment and considerations for application of the interferometer.

The preliminary alignment procedures suggested in Section 4 B usually are not precise enough to obtain an oscilliscope presentation of the quality required for accurate spectral analysis of the laser output. Once the oscilliscope presentation is obtained, however, additional adjustment of the alignment controls while observing the effects on the oscilliscope, provides the necessary means for achieving final perfection in the SFPI alignment.

After a brief description of the general nature of the spectral output of lasers, two particular application considerations are described which are required for optimum spectral analysis results.

The spectral output of lasers [23] consists of an ensemble of axial modes or oscillations the number, spacing, and amplitude of which is de-

[7] The FM Laser System is discussed in further detail in Section 7. The KDP (potassium dihydrogen phosphate) electroptic modulator requires a pulsed form of modulation in order to achieve peak power requirements while conforming to the average power limitations of the crystal.

termined primarily by the laser cavity resonances that independantly saturate the Doppler-broadened flourescent line. A typical spectrum is shown diagramatically in Fig. 17. The Doppler width of the line is approximately 1500 Mc/s. The free spectral range for the laser resonator is given by c/2L. Two particular considerations on which we shall comment are (1) the requirement for selective mode excitation in the laser and (2) the requirement that the SFPI free spectral range be properly chosen to avoid ambiguity in the output information presented on the oscilliscope.

(1) For optimum spectral analysis of the laser output, the laser should be operating in the fundamental TEM_{00q} mode. This will insure that higher order modes which may be present in the laser radiation and subsequently in the SFPI output, are not mistaken as a misalignment indication and cause undue effort and delay while attempting to improve the oscilliscope presentation. A Gaussian intensity distribution in the far field usually [24] indicates that the TEM_{00q} mode of laser operation has been achieved. If any doubt exists, a direct check of the laser RF beat frequency spectrum with a photomultiplier and RF spectrum analyser should reveal any significant higher order modes, if present.

(2) To conduct an accurate examination of the laser mode spectrum a suitable choice of SFPI free spectral range must be made. Sufficient clearance must be provided between the oscilliscope presentations, which are periodic, in order to resolve the axial modes present in the laser output. Additional clearance is required in the event the laser output spectrum contains modulation sidebands. Whenever the SFPI free spectral range is less than the Doppler broadened floresence line, as

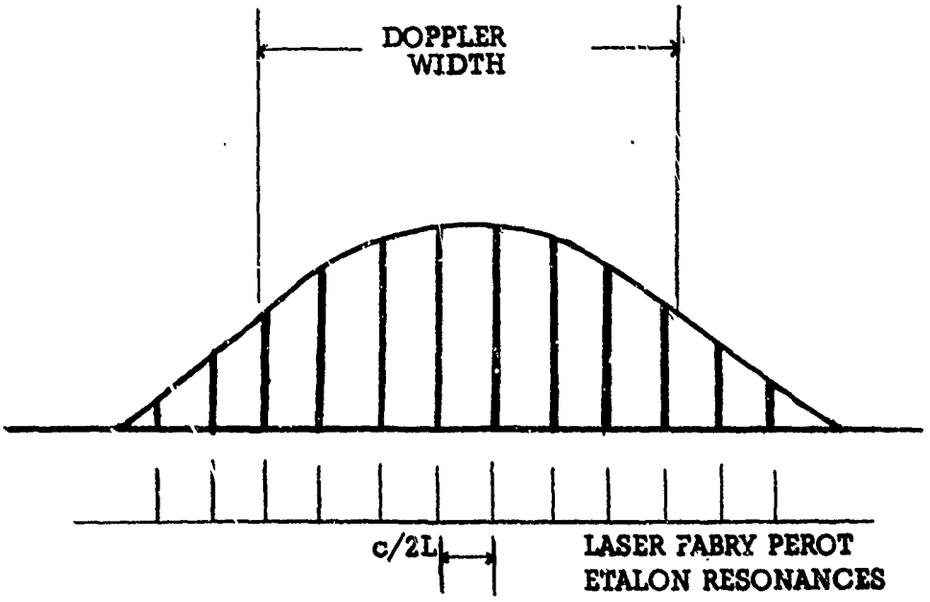

Fig. 17 A typical laser mode spectrum showing the Doppler broadened line width and the Fabry Perot etalon resonances spaced by c/2L.

shown in Fig. 18a the resultant oscilliscope display contains overlapping axial modes as shown in Fig. 18b. A choice of SFPI reflector separation greater than 10 cm can cause this ambiguity problem in the oscilliscope display, since c/2L is 1.5 Gc/s for L=10 cm, which is the assumed value for the laser Doppler broadened line. In certain instances greater resolution may be required and the display ambiguity must be considered carefully for accurate analysis of the desired information. When the laser output spectrum contains modulation sidebands, the SFPI reflector separation should be chosen to provide clearance on both sides of the Doppler broadened line. Fig. 19 shows a diagram of a typical display resulting from a proper choice of SFPI mirror separation for studying a 1.25 Gc/s amplitude modulated laser with five axial modes present. L_I chosen in this case was 4 cm, which gives a SFPI free spectral range c/2L of 3.75 Gc/s which is sufficient to prevent display overlap for this modulation frequency. Laser mode frequency spacing is shown as $c/2L_L = 250$ Mc/s.

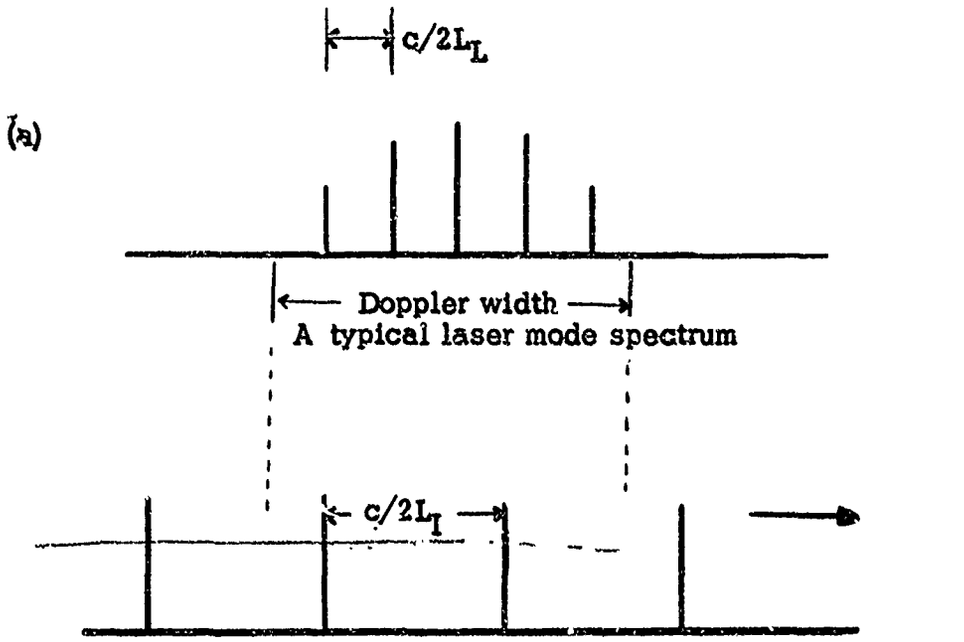

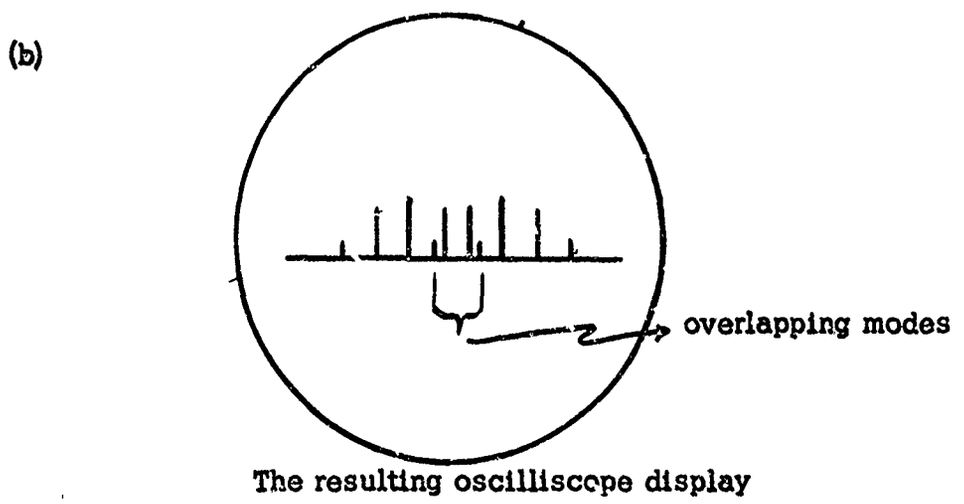

Fig. 18 a. A diagram showing the scanning interferometer resonances separated by $c/2L_I$, less than the Doppler broadened gain curve.

b. The resulting oscilliscope display with overlapping mode spectra.

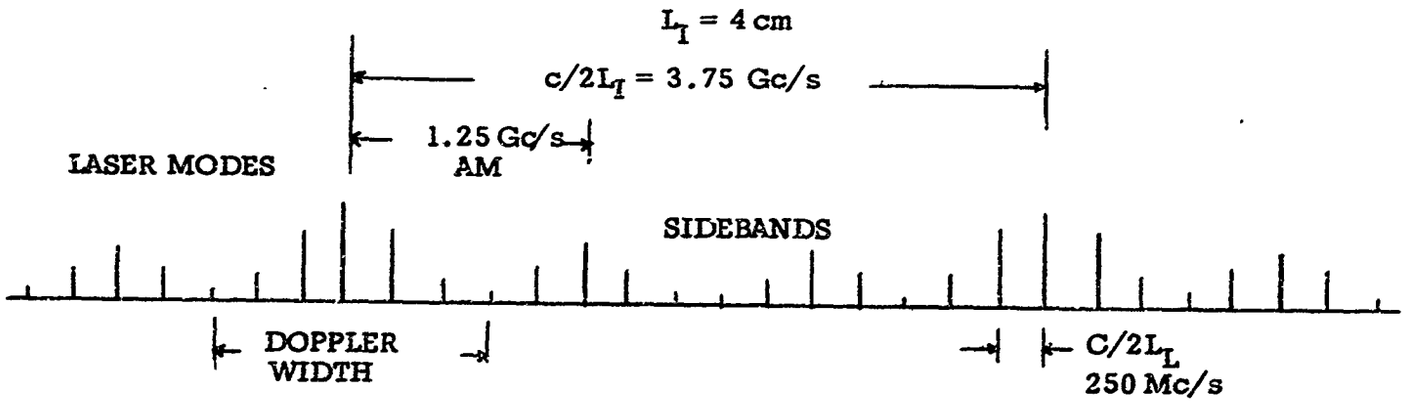

Fig. 19 A diagram of the oscilliscope display when the spacing of the interferometer mirrors is correctly chosen to allow for modulation sideband information. Amplitude modulation at 1.25 Gc/s is shown with the required mirror spacing of 4 cm or less giving the necessary clearance to prevent overlapping of the modes.

5. Experimental Evaluation of the Scanning Fabry Perot Interferometer

A. Method of evaluation and arrangement of the system.

Experimental evaluation of the SFPI included:

(1) A check of the alignment procedures and controls;

(2) Application of the matching procedures; and

(3) A comparison of the output characteristics of the SFPI with the theoretical results of Section 2. The results of these evaluations are contained in parts B. C. and D. of this section, respectively.

The initial experimental arrangement is shown in Fig 20. A Spectra Physics model 131 gas laser, operating with a hemispherical resonator, provided approximately .5 mw of optical power in the TEM_{00q} mode. This output beam was passed through an isolating polarizer and quarter-wave plate combination and was matched to the SFPI by a double lens system positioned according to the matching conditions of Case II. The SFPI receiving mirror was scanned by the PZT-4 transducer which was driven by the variac and line transformer combination voltage source. The output radiation from the SFPI was detected by an RCA 7102 model photomultiplier and displayed on a Tektronix 531 oscilliscope. Horizontal deflection of the oscilliscope was synchronous with the piezoelectric mirror scan.

B. Alignment procedure and evaluation of control performance

Accurate and precise fabrication of the SFPI[8] insured excellent alignment of the basic structure with minimum adjustment necessary for operation.

[8]By Mr Lyle Wishart of Sylvania Electronics System

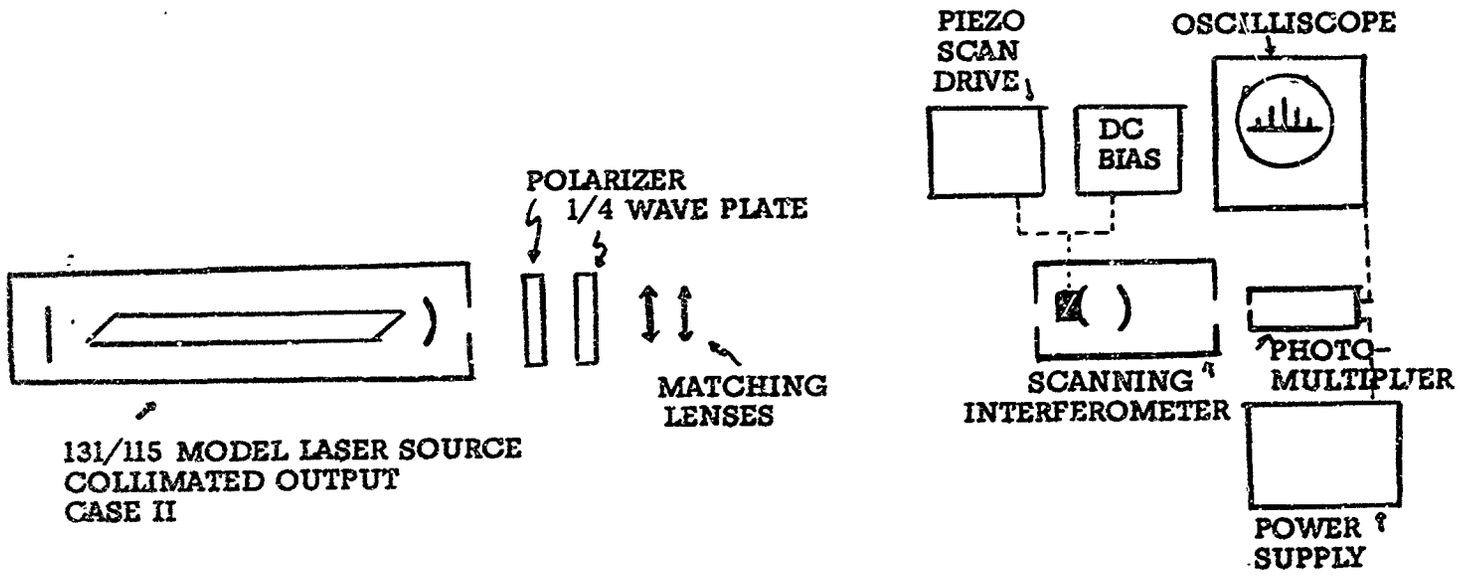

Fig. 20 A schematic arrangement of the experimental apparatus required for Case II application of the scanning interferometer.

Vernier controls of the rear mirror alignment were centered by changing the basic support angle of the rear mirror mounting disc.[9] Improved response of the rear mirror vernier controls was obtained by freeing the control plungers and tightening the mounting disc retaining spring tensions. The PZT-4 transducer was initially shimmed slightly at the base to correct an axial misalignment caused by an error in the flatness of the transducer at the mirror interface. No discernable improvement resulted from this procedure, however, and the shim was subsequently removed. The piezoelectric scan was measure and found to be within one per cent of the manufacturer's specification, viz., approximately 880 A° per 100 volts applied voltage throughout a scanning range in excess of three half-wavelengths. Oscilliscope displays of greater than three half-wavelengths scan without off-axis distortion, gave visual verification of the coaxial motion of the scanning mirror.

Alignment procedures outlined in Section 4 B were a successfully followed for all applications of the SFPI in this paper. Response to controls was excellent with no discernable backlash, and a high degree of sensitivity. Alignment stability is greatly dependent on the application environment. Of particular importance is the requirement for isolation of the SFPI and matching lens components from physical disturbance which necessitates realignment. After initial, precise alignment, only very minor adjustment of position controls was required for typical applications

[9] A small ball bearing provides a replaceable pivioting seat at the base of the rear mirror mounting disc, held fast by the disc retaining spring tension. In the rear mirror is seated slightly askew with respect to the axis, this bearing may be replaced as an alternative to reseating the mirror in its mount at a better angle.

of the SFPI such as in the FM Laser Program study.

Drift of the entire oscilliscope display was greatly effected by air currents between the SFPI mirrors, and by ambient temperature variations which changed the SFPI mirror separation. These effects were mitigated by a plexiglass enclosure, which also reduced short term frequency fluctuations in the SFPI output caused by local noise. Temporary drift of the oscilliscope display is easily compensated for by application of a suitable DC voltage to the transducer as a bias to center the mirror scan. A typical result of SFPI output distortion caused by mechanical vibrations and microphonics is shown in Fig. 26a, (p. 54). High speed photo techniques with exposure times 0.02s or better eliminate most of the undesirable fluctuations caused by environmental disturbances. For optimum performance and results the SFPI and matching components must be located on a stable platform.

C. Evaluation of the matching procedures

The matching procedures described in Section 3 C for Case II were successfully applied to the collimated beam radiated from the hemispherical resonator of the 131 model laser. A practical method of application of these matching procedures is suggested as follows: A double lens system is used to achieve the required focal length $f = f_o$. After setting the double lens system and the SFPI according to the calculated value of the characteristic length f_o, the lens closest to the laser is moved to vary the position of the beam focus to a point inside the SFPI a distance Z_I from the receiving mirror. Accomplishment of this focus is observed

by holding a card inside the SFPI cavity at the required focal point, and varying the lens position until the minimum spot is achieved. Some difficulty is encountered if the double lens system is not stably placed on a suitable small optical bench. The traversal of the matching lens must remain coaxial with the laser beam as the lens is adjusted. Observation of the oscilliscope display is of assistance in subsequent adjustment of the optimal position and focussing of the double lens system. The oscilliscope display also gives an indication of the extreme criticallity of this particular phase of the alignment and matching procedure. Appendix I, Table I contains a summary of the results of the applied procedures for matching the SFPI to the 131 model laser output for SFPI spacings L_I=5, 7, 11, and 14 cm.

D. Observed characteristics of the interferometer

It was found that the 131 model laser output consisted of three axial modes separated by 500 Mc/s. The frequency spacing of the modes is determined by the length of the laser cavity, which is L_L= 30 cm for this model laser. This frequency spacing was verified by an RF beat frequency spectrum analysis of the output of a photomultiplier with direct detection of the laser beam. This axial mode frequency separation was subsequently used as a convenient calibration for the oscilliscope display by aligning the axial modes with the desired oscilliscope scale markings. The limited number of axial modes oscillating in the 131 model laser makes it an ideal source for initial experimenting and for the purposes of familiarizing oneself with the matching and alignments of the SFPI.

The first observations made of the laser mode spectrum revealed that the half intensity width $2\delta\nu$ and consequently the finesse $\mathcal{F}$ and resolution of the SFPI were considerably below anticipated requirements. Conclusion was immediately made that mirror reflectivity was not the 99 per cent desired. According to a half-intensity width $2\Delta\nu$ of approximately 40 Mc/s, (L_I=7 cm) and to values plotted in Fig. 5, the true reflectivity was determined to be only 95%.[10] A new pair of reflectors was subsequently installed. The measured light intensity transmission loss for these mirrors was approximately one per cent, which when combined with absorbtion and scattering losses, yields a mirror reflectivity of approximately 98.5 to 98.7%. Figs. 22a and b give a clear indication of the improvement in resolution achieved, and the critical dependance of this resolution on the requirement for high values in mirror reflectivity.

Fig. 21a shows a typical output spectrum of the Spectra Physics model 131 laser, when proper matching and alignment is achieved, while Fig. 21b shows the effect of misalignment or improper matching. Fig. 23 shows the variation in individual mode amplitude caused by thermal effects on laser cavity dimensions. The laser modes are seen to drift across the Doppler broadened flourescent line as the central cavity resonance frequency changes with resonator dimensions.[11]

[10] This figure was verified by a direct reading on a power meter. Reflector light intensity transmitted was greater than 4% of the input. This value combined with absorbtion and scattering losses yields a mirror reflectivity approximately the 95% value determined above.

[11] A brief study of this long term frequency drift is presented in Section 6, using the greater number of more closely spaced modes in the output of a 115 model laser.

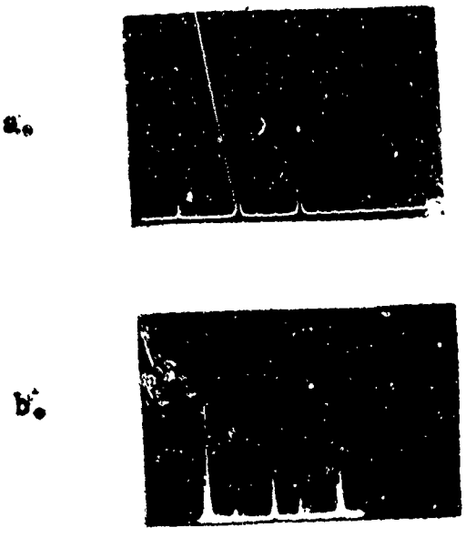

Fig. 21 Spectra Physics model 131 laser modes
c/2L ≈ 500 Mc/s
(a) SFPI properly aligned and matched to laser
(b) SFPI missaligned and not matched to laser

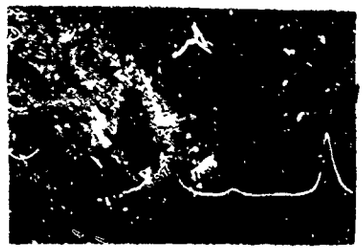

R .955
Scale: 100 Mc/s per division horizontal
$2\Delta\nu \sim 40$ Mc/s

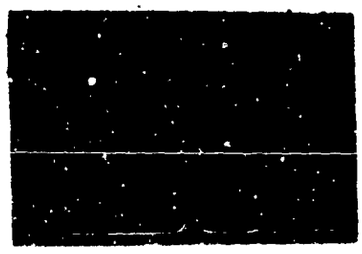

R .985
Scale: 50 Mc/s per division horizontal
$2\Delta\nu \sim 10$ Mc/s

Fig. 22 Improvement in resolution with increase in mirror reflectivity R

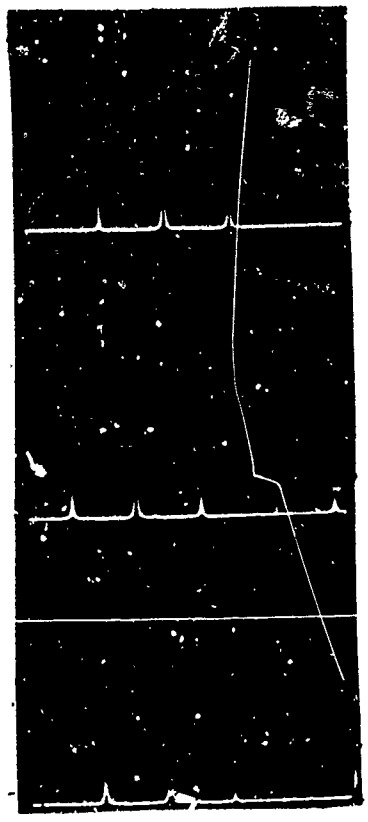

Fig. 23 Spectra Physics 1-1 model laser mode amplitude variation caused by thermal effects on laser cavity length

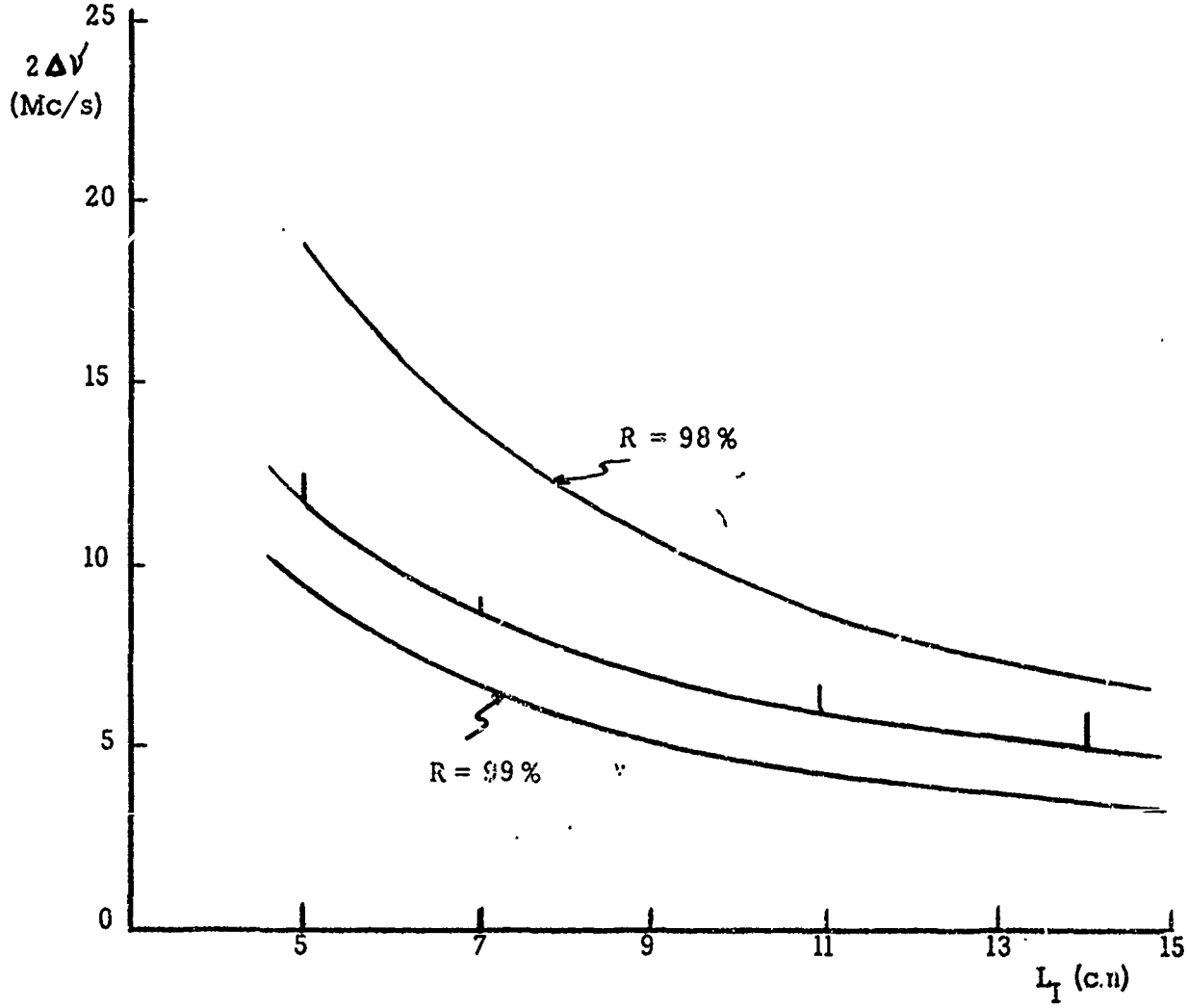

Fig. 24 Experimental observations of the interferometer half-intensity width $2\Delta\nu$ vs. mirror separation L_I. Theoretical values for R = 98% and 99% are shown for comparison.

Photographic data was taken to determine the half-intensity width for SFPI mirror spacings of 5, 7, 11 and 14 cm. The values obtained for $2\Delta\nu$ at these points is shown in Fig. 24, with excellent agreement with the theoretical values of Fig. 5 Section 2. The tendency for half-intensity width $2\Delta\nu$ to be slightly greater than theoretical values, especially as SFPI mirror spacing is increased, is attributed to deviations of matching and alignment from optimum requirements. For each particular SFPI mirror separation, new positions for the lens and the SFPI were required, according to proper matching procedures, in order to achieve the maximum resolution capability of the instrument. In normal application situations only one setting of the SFPI mirror spacing is used during experimentation, and the matching arrangement once established does not change. Improvement in half intensity width $2\Delta\nu$ by as much as 10 per cent was realized when the lens system and SFPI were properly relocated for each new setting of the SFPI mirror spacing L_I, during this particular phase of evaluation.

Variation of the SFPI mirror spacing L_I resulted in a change in the free spectral range which was observed to be in exact agreement with expected values of $C/2L_I$ shown in Fig. 3 for all spacings used. As shown in Section 2 D, the ratio of the SFPI free spectral range ν_{fsr} to the half intensity width $2\Delta\nu$ determines the SFPI finesse $\mathcal{F}$. The finesse $\mathcal{F}$ achieved was found to be between $\mathcal{F} = 230$ to 264 which is also in agreement with the values shown in Fig. 4 based on a mirror reflectivity estimate of approximately 98.5 to 98.7%. Typical photographs used in determining the half-intensity width $2\Delta\nu$ are shown in Figs. 25 a,b and c.,

$L_I \sim 7$ cm, $2\Delta\nu \sim 9.5$ Mc/s

$L_I \sim 11$ cm, $2\Delta\nu \sim 7.5$ Mc/s

$L_I \sim 14$ cm, $2\Delta\nu \sim 5$ Mc/s

Fig. 25 Variation of half-intensity bandwidth $2\Delta\nu$ with SFPI mirror spacing L_I

a.

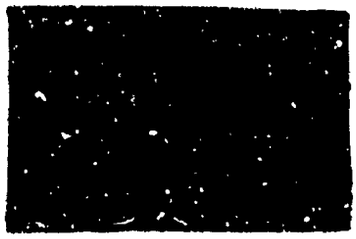

b.

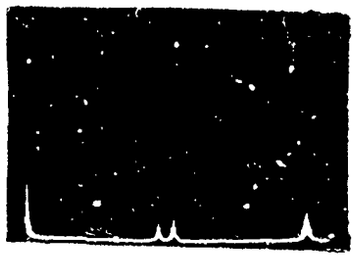

c.

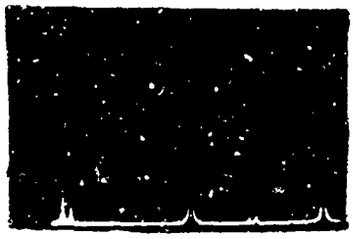

Fig. 26 SFPI output distortion caused by
(a) mechanical vibrations and microphonics
(b) SFPI free spectral range being approximately the same as the Doppler linewidth

with SFPI mirror separations L_I of 7, 11, and 14 cm and half-intensity widths $2\Delta\nu$ observed as 9.5, 7.5, and 5 Mc/s respectively.

In the process of taking data for evaluation of the half-intensity width $2\Delta\nu$ the SFPI mirror spacings of 10 cm and 15 cm were avoided since the free spectral range of the SFPI would then have been a multiple of the laser mode separation and an ambiguous oscilliscope display results. This ambiguity was previously discussed in Section 4 D. Figs. 26b and c show a situation where two modes on the display are almost superimposed and it becomes difficult to obtain an accurate calibration because the proper selection of laser modes is not readily apparant.

E. Summary

We now have a clear indication of the performance of the SFPI from experimental observations which are in excellent agreement with theoretical values. The same type of optical resonator which provides for the successful operation of lasers also affords us with a means for studying the laser's output. A piezoelectric scan of the passive SFPI resonance across the laser output band of frequencies provides a highly resolved display of the laser spectral characteristics for visual study and analysis.

6. Frequency Stability Study of the Spectra Physics Model 115 Laser.

A. Introduction and background

The SFPI was applied to the study of long and short term frequency stability characteristics of a 115 model gas laser under environmental conditions as described below. Additional experience with the matching and alignment procedures was also acquired during experimentation with this laser.

Although no final standard has been set for frequency stability of lasers, measurements have been made by Javan and others [26] using two CW, He-Ne gas lasers with improved mechanical stability and adjusted to oscillate in only one mode. These measurements were made by RF beat frequency spectrum analysis obtained "under typical Bell Telephone Labratory conditions". It was found that a long term frequency drift of 0.5 Mc/s per 100 s occurred which corresponds to two parts in 10^9 for the 1.153 micron transition. This long term frequency stability is effected by thermal and mechanical variations of the laser Fabry Perot etalon spacing, and is therefore dependent on the environment in which the measurement is made. The sensitivity of this dependence is well illustrated by the fact that, for the Spectra Physics 115 model laser, a minute change in reflector spacing of 12.5 A° caused by ambient temperature or other variations, causes a change of approximately one Mc/s in the frequencies of the output modes.

B. Purpose and methods of experimental observations

The purpose of this experiment was to apply the SFPI to a study of long term laser mode drift in order to compare the drift under varying

environmental conditions. In addition, the SFPI was applied to observe the decrease in mode drift from initial light-off until a steady state operation is established in order to determine a required warming time before a steady state drift is established.

The SFPI provides a more direct method for measuring frequency drift and short term fluctuations in the laser output than that of Javan decribed above. By observing the variation of the amplitude of a particular mode as it drifts across the Doppler broadened flourecence line and relating the change in amplitude to the known axial mode frequency separation, a direct measure of laser frequency drift is obtained. Presentation of the SFPI output on the oscilliscope revealed three situations for use as criteria for mode drift measurement by this direct method.

(1) A measurable time elapses between the generation of two consecutive modes above threshold for oscillation.

(2) A measurable time elapses between the decay of two consecutive modes below threshold for oscillation

(3) A measurable time elapses between the attainment of maximum amplitude (center of the Doppler broadened line) by two consecutive modes.

Using any one of these measured times, and the fact that the axial mode separation for the 115 model laser is 250 Mc/s (based on a reflector separation of 60 cm), a laser mode drift may easily be obtained from direct visual observation. No particular variation was observed in using any or all of the above criteria for the experimental determination of the laser mode drift. Measurement of short term frequency fluctuations, using the

SFPI, is by direct high speed photographs of the oscilliscope display of the mode frequency fluctuations caused by vibration, microphonic, and noise effects.

C. Experimental arrangement

The arrangement of experimental apparatus for the laser frequency stability studies was as shown in Fig. 20 p. 43. The more versatile 115 model laser was used in place of the 131 model. The 115 model laser operating with a hemispherical resonator (Case II, on p. 18) provided a collimated output the power and mode content of which could be power supply and mirror position adjustment. Appropriate matching conditions for this case are summarized in Table I, Appendix I. During the matching phrase of this experiment, a particular off-axis mode in SFPI output could not be eliminated by careful alignment efforts. The usual off-axis interference and clutter was elimated, but despite all effort, distortion remained in the oscilliscope display. A direct check of the laser output by RF beat frequency spectrum analysis revealed a 15 Mc/s beat note in the analysis of the laser output. This verified that the distortion, in the SFPI output was not caused by misalignment or imporper matching, but by a higher order transverse mode in the laser radiation.[12] This observation emphasizes the complementary use of the SFPI and the RF spectrum analyser in this respect. The number of modes in the laser output varied from seven at 4.5 milliwatts to four at 1.7 milliwatts output power with the laser operating

[12]Mode impurity in the output of the 115 model laser has been studied by Heinemann and Redlien [24] who observed that the Gaussian intensity distribution in the laser output does not always indicated achievement of the TEM_{00q} mode of laser operation.

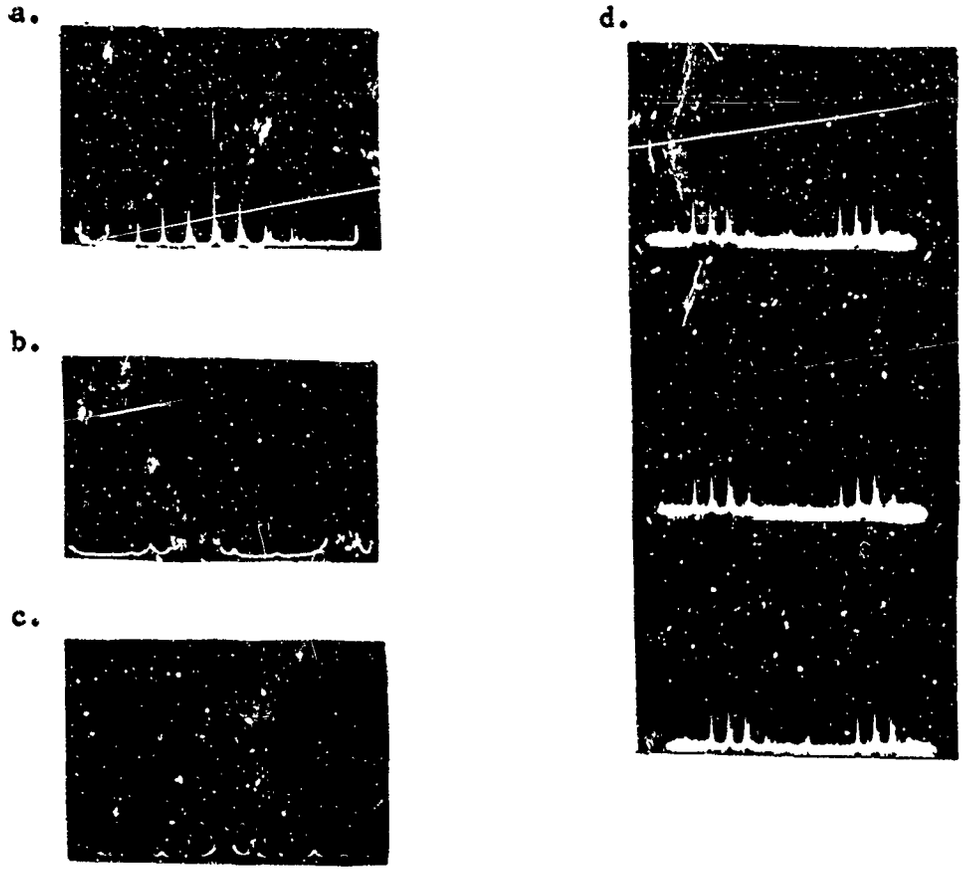

Fig. 27 (a) Distortion in Spectra Physics model 115 laser spectrum when not in TEM_{00q} mode; $c/2L \approx 250$ Mc/s

(b) Expanded view of (a);Scale: 50 Mc/s per division horizontal;Note the frequency fluctuation caused by short term vibration effects

(c) Short term instability in frequency ν and amplitude A $\Delta\nu = \pm 5$ Mc/s ; $\Delta A = \pm 5$ per cent; T = 0.04 s

(d) Variation in mode amplitude caused by long term frequency drift; T ~ 30 s between each view

in the TEM_{00q} mode. A maximum power of 5.6 milliwatts (eight modes) had been observed, but there was excessive higher order mode interference in the laser radiation. This is shown in Fig. 27 a and b. The distortion was reduced by adjustment of the controls for laser mirror alignment to achieve TEM_{00q} mode of operation.

The SFPI was situated inside a plexiglass box enclosure, as previously mentioned in Section 5 B, and covered with a large plastic cloth. This protection eliminated a slow drift in the entire oscilliscope pattern usually caused by such effects as drafts in the SFPI cavity or ambient temperature variations in the SFPI mirror spacing. Vibration effects, such as microphonics, were reduced, but mechanical vibrations still caused occasional fluctuations in the SFPI resonances. The short term effects had no noticible effect on the long term frequency drift observed.

D. Experimental observations

(1) An observation of the laser mode drift was made at night in a typical laboratory space with doors closed and normal equipment functioning for experimental requirements. The laser was lighted off and drift recorded during a period of three hours to determine the length of the time required to establish an equilibrium or steady state drift. The results of this experiment are shown in Fig. 28. The laser presented four modes for observation with a power output from 1.7 milliwatts to 1.8 milliwatts. A steady state drift condition, where the mode drift is no longer attributed to the thermal effects of the laser warming up, was achieved in approximately 90 minutes. The drift was determined to be less than 1.4 Mc/s per 180s. Fig. 21 d shows a typical observation of the mode amplitude variation which was used for drift measurement. The sequence was taken at 30 second intervals

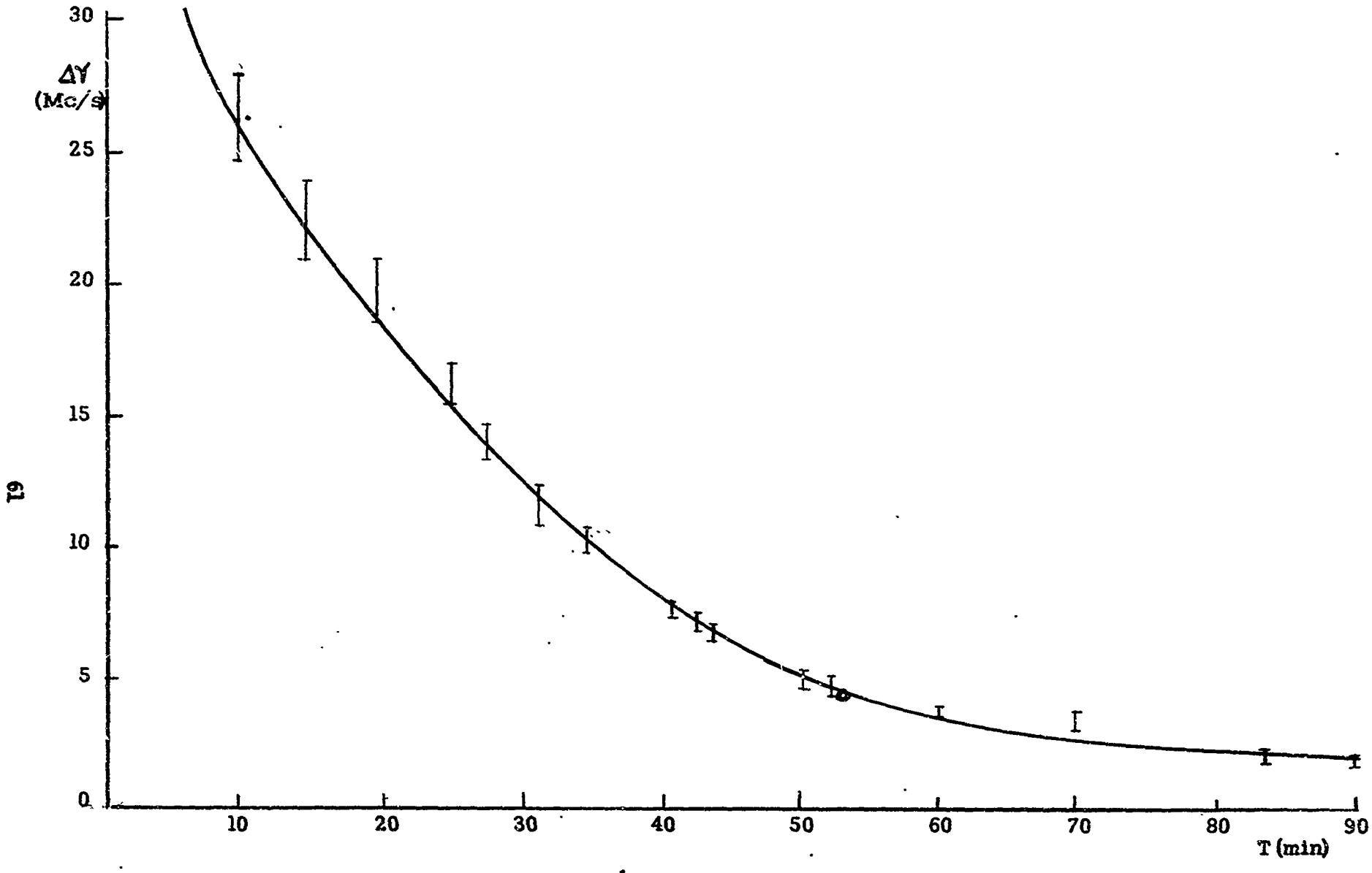

Fig. 28 A typical frequency drift $\Delta\nu$ of the laser modes vs. time elapsed T from initial light-off.

and shows a pattern repetition or total frequency drift of 250 Mc/s has almost occurred. Drift in the sequency was to the right across the Doppler line display, as indicated by the growth of the left mode as it nears the center of the Doppler line. The elapsed time for this particular observation was subsequently recorded as 65 seconds resulting in a drift of 3.85 Mc/s per 65s. The observation was taken at time 0 + 52 minutes and is circled in Fig. 26.

(2) Additional observations of laser mode frequency drift were obtained under varying laboratory conditions with the results as low as 2.5 Mc/s in a closed laboratory in the daytime to 5 Mc/s drift during normal working conditions. Long term frequency drifts as high as 10 Mc/s were recorded during sudden environmental changes or variations in the laser power level. Steady state conditions were subsequently regained in a period of from 15 to 45 minutes depending on the type of variation which originated the disturbance. Fig. 29 shows a typical drift variation caused by a reduction the laser power level from 4.5 milliwatts to 1.8 milliwatts output.

(3) Short term mechanical vibrations and noise caused fluctuations in the frequencies and amplitudes of the modes presented in the SFPI output. These fluctuations are caused by a combination of both the SFPI and the laser reflector vibrations, and cannot be attributed to the laser characteristics alone. Under varying laboratory conditions ranging from quiet night to normal working conditions, the intermittant fluctuations ranged from 1Mc/s to as much as 10Mc/s and the mode amplitudes of the modes presented in the SFPI output. These fluctuations are caused by a combination of both the SFPI and the laser reflector vibrations, and cannot be attributed to the laser characteristics alone. Under varying laboratory conditions ranging

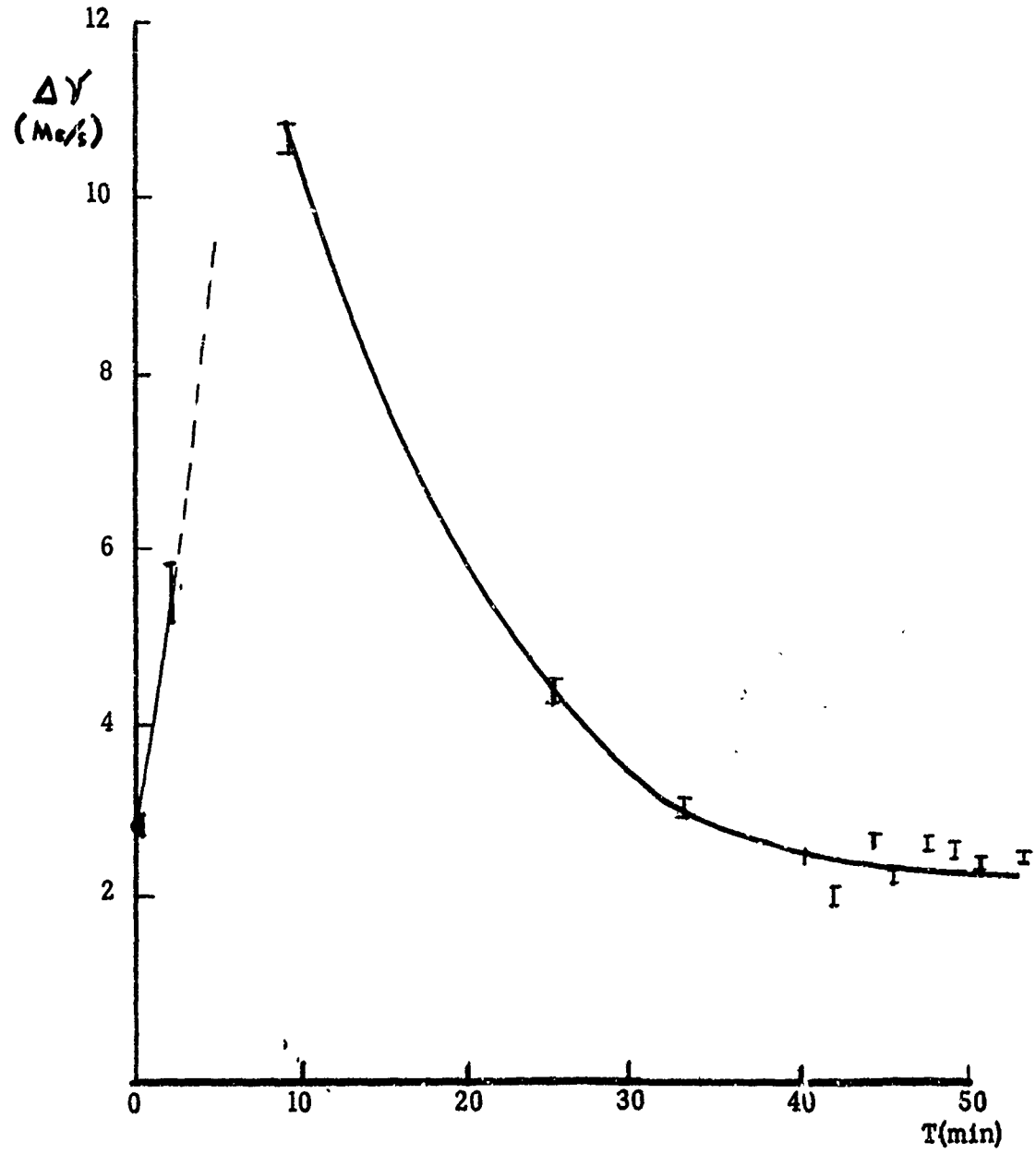

Fig. 29 A typical laser mode frequency drift $\Delta\nu$ vs. T caused by a reduction in laser power output from 4.5 to 1.8 milliwatts.

from quiet night to normal working conditions, the intermittant fluctuations ranged from 1Mc/s to as much as 10Mc/s and the mode amplitudes of the well formed center modes in the Doppler broadened line varyed from 5 percent to as much as 30 percent. A typical observation of the rapid mode fluctuations is shown in Fig. 27 c, with T = 0.04 s. $\Delta\nu \pm 5$Mc and ΔA = ± five per cent.

E. Summary and conclusions for Section 6

The most effective use of the SFPI for any frequency characteristic study, such as stability, dictates that the instrument be isolated from all environmental disturbances which might superimpose SFPI instabilities onto the laser instabilities. Long term frequency drift is much less affected since the method used in this section is dependent on only the relative amplitude variations of the laser modes as they drift across the Doppler broadened line. Rapid fluctuation studies require an extremely stable platform for the SFPI with respect to the laser platform in order that any fluctuations may be attributed to the laser itself. This may be quite difficult in instances where the laser is also situated on a stable platform. A conclusion is made from experimentation that a laser requires a definite stabilizing period after light-off for equilibruim in long term frequency stability. In addition any environmental variations or power changes also require a stabilizing period for the laser to regain a steady state operation.

7. Application to the FM Laser program

A. Introduction

The most interesting aspect of the work completed at the Electronic Defense Laboratories, was an application of the SFPI to a study of the spectral characteristics of the FM Laser [9]. After a brief background discussion in part B, the basic principles and operation of the FM Laser are discussed in detail in part C in order to clarify the results obtained from the application of the SFPI in the program. Experimental application of the SFPI is then described in part D. Photographic results are presented as an indication of the various spectral outputs of the laser during the FM Laser experimental studies, and as emphasis of the improved resolution and value of the SFPI constructed for this program.

B. Background

One of the significant problems encountered in the development of an effective, working optical communications system, employing optical heterodyne receivers, has been the need for well defined mode control of the multimode operation of the lasers used. [12] This need arises from the nonlinear interactions between the multiple oscillations of free running lasers when used as optical carriers or local oscillators. The randomly phased oscillations produce multiple beats when mixed in a square-law photodetector. The majority of these beats are considered undesirable noise which interferes with or even obscures the signal received. These problems had previously rendered the laser ineffective as an optical carrier or local oscillator.

The FM Laser is the result of a new technique of mode control developed to eliminate these problems. Instead of operating the laser in a low power single mode fashion to eliminate the multiple interfering beats, a new technique assigns amplitudes and phases to the free running laser modes, which causes the multimode output to have the spectrum of a frequency modulated (FM) signal, hence the resultant FM Laser. The FM Laser modes have amplitudes and phases of an FM signal and when mixed at a photodetector with another signal no longer produce the undesirable multiple beat effects because of the phase characteristics of FM sideband pairs. The FM Laser is therefore available for use in heterodyne receivers as a local oscillator or as a signal carrier with all the power of the now well defined and controlled modes, and without the undesirable multiple axial mode beats (noise) when detected with a photomultiplier.

C. Principles of the FM Laser and initial experimental operation

(1) The principles and initial operation of the FM laser is best described in the original artical by Harris and Targ where they reported: [6]

"the operation of a He-Ne laser in a manner such that all of the laser modes oscillate with FM phases and nearly Bessel function amplitudes, thereby comprising the sidebands of a frequency modulated signal. The resulting laser oscillation frequency is, in effect, swept over the entire Doppler line-width at a sweep frequency which is approximately that of the axial mode spacing. This type of FM oscillation is induced by an intracavity phase perturbation which is driven at a frequency which is approximately, but not exactly, the axial mode spacing. Experimental evidence supporting the hypothesis of an essentially pure FM oscillation is as follows:

1. The suppression of all observable laser "beat notes" by at least 25 dB, as compared to their value in the absence of the phase perturbation. A 5 % increase in laser power was observed coincident with this suppression.

2. The observation of a scanning interferometer showing the laser modes to possess approximately Bessel function amplitudes, appropriate to the spectral components of a pure FM signal.

3. Direct demodulation of the resultant FM signal using both a Michelson interferometer and a birefringent discriminator. [26]

The laser was a Spectra-Physics Model 116 operated at 6328 A° with an external mirror spacing corresponding to an axial mode interval (c/2L) of 100.5 Mc/sec. The phase perturbation was obtained via the electro-optic effect in a 1-cm long KH_2PO_4 (KDP) crystal which was anti-reflection coated and situated in a 100-Mc/sec tuned circuit inside the laser cavity. The KDP crystal was oriented with its optic axis parallel to the axis of the laser tube, and with one of its electrically-induced principal axes parallel to the direction of the laser polarization. A KDP crystal in this orientation introduces a pure phase perturbation and ideally should introduce no time varying loss into the laser cavity. An rf input power of 2 W produced a single-pass phase retardation δ of about 0.66 rad at the optical frequency.

Of particular interest was that FM laser oscillation was not obtained when the KDP modulator was tuned exactly to the frequency of the axial mode spacing. In this case, the laser beat notes as observed on an rf spectrum analyser were stabilized and enhanced, and appeared similar to those described by Hargrove and others, [27] and DiDomenico [28] in their papers on AM phase locking.

When the modulation frequency is detuned from the c/2L frequency then at a δ of 0.05, a frequency change of 250 kc/sec to either side produces an abrupt quenching of all of the original laser beat notes, with a coincident increase of 5 % in the total laser oscillation power. This removes the possibility that the quenching of the axial mode beats is caused by some form of increased optical loss. After quenching of the original axial beat notes, a small amount of rf beat power may be observed at harmonics of the modulation frequency. At the second and third harmonics, this power level was 25 dB below that of the original beat amplitude. At the fundamental and fourth harmonics, this level was at least 15 dB below that of the original signal. Measurements at the latter two frequencies were limited by a residual AM light signal and poor photomultiplier sensitivity, respectively.

In order to directly verify the presence of an FM signal, the output of the FM laser was passed through an optical discriminator (Michelson interferometer) with a path length difference of 30 cm. The interferometer was followed by a photomultiplier and rf detector. With both arms of the interferometer open, a strong signal at the modulation frequency was observed with a 15 dB signal-to-noise ratio. If either arm of the interferometer was blocked, this signal completely disappeared.

The most interesting and perhaps startling results of our experiments were obtained by direct observation of the laser mode amplitudes with a Spectra-Physics scanning interferometer. In the absence of modulation, the laser modes appear as in ..... Fig. 33 A .....[13]. As the modulation depth is increased, the central mode amplitude begins to fall, the first pair of sidebands increase. At still larger δ's the second and third pair of sidebands achieve significant amplitudes, and there is a diffusion of power toward the wings of the Doppler line. Examination shows the modes to have approximately Bessel function amplitudes, which are not determined by independent saturation of the Dopper line, as might have been expected. ..... Figs. 33 B through E .....[13] are captioned in terms of both the depth of the single-pass modulation and also in terms of the depth of the frequency modulation on the output signal of the FM oscillator. This latter modulation depth is denoted by Γ, and from the varying frequency viewpoint of frequency modulation, it is the ratio of the peak frequency deviation to the modulation frequency. The ratio of Γ/δ, that is the ratio by which the modulation process is enhanced by the presence of the cavity and the active media is 40. Alternate measurements of Γ were made using the Michelson interferometer, and similar results were obtained. Our highest measured Γ was 6, which at a modulation frequency of 100 Mc/sec corresponds to a peak-to-peak frequency swing of 1200 Mc/sec. .....".

(2) A quasi-static model [12] of the effect of the internal modulation describes the generation of the FM Laser output spectrum. Phase modulation of the original modes of the free-running laser positions FM sidebands in the vicinity of these modes. These sidebands are slightly offset in frequency from the laser modes by a chosen amount of detuning

[13]Figs. 33 A and 33 B through E are sample improved versions of similar presentations referenced in the original article.

from the original axial mode frequency separation(c/2L)[14] These sidebands, in effect stimulate emission out of the same portion of the Doppler broadened flouresecent line as the laser modes, and therefore, when their amplituded are sufficiently high burn a sufficient hole [29] to quench the neighboring original laser modes. Thus the FM sidebands with their own well defined phases [30], and their amplitudes defined by Bessel function distributions rather than by saturation of the Doppler broadened flouresecent line. The sidebands originate by internal phase modulation and hence are parametric or driven oscillations, and can be considered as the quenched original axial modes at new locations. Thus the process has been decribed as parametric regeneration. [9]

Fig. 30 shows a diagram of the spectrum of the modes when the laser is free-running and when internal modulation has been applied at a frequency detuned 0.1 Mc/s from the fundamental mode beat frequency of 100 Mc/s. Also shown in Fig. 30 is the orientation of the internal modulator with respect to the laser polarization for the phase perturbation introduced in the cavity. Fig. 31 b shows an oscilliscope presentation of a

[14]If the modulation introduced in the cavity is synchronous with the axial mode spacing, C/2L, the resulting laser output is an ensemble of axial modes coupled with well defined amplitudes and phases. The SFPI output shows that a stabilization or locking has changed the rapidly fluctuating mode intensities to a stationary spectrum. This locking phenomenon is described by Hargrove and others [27] and analysed by Di Domenico [28]. The AM locked laser although not advantageous in the manner that the FM laser is, may well prove useful in other respects yet to be determined.

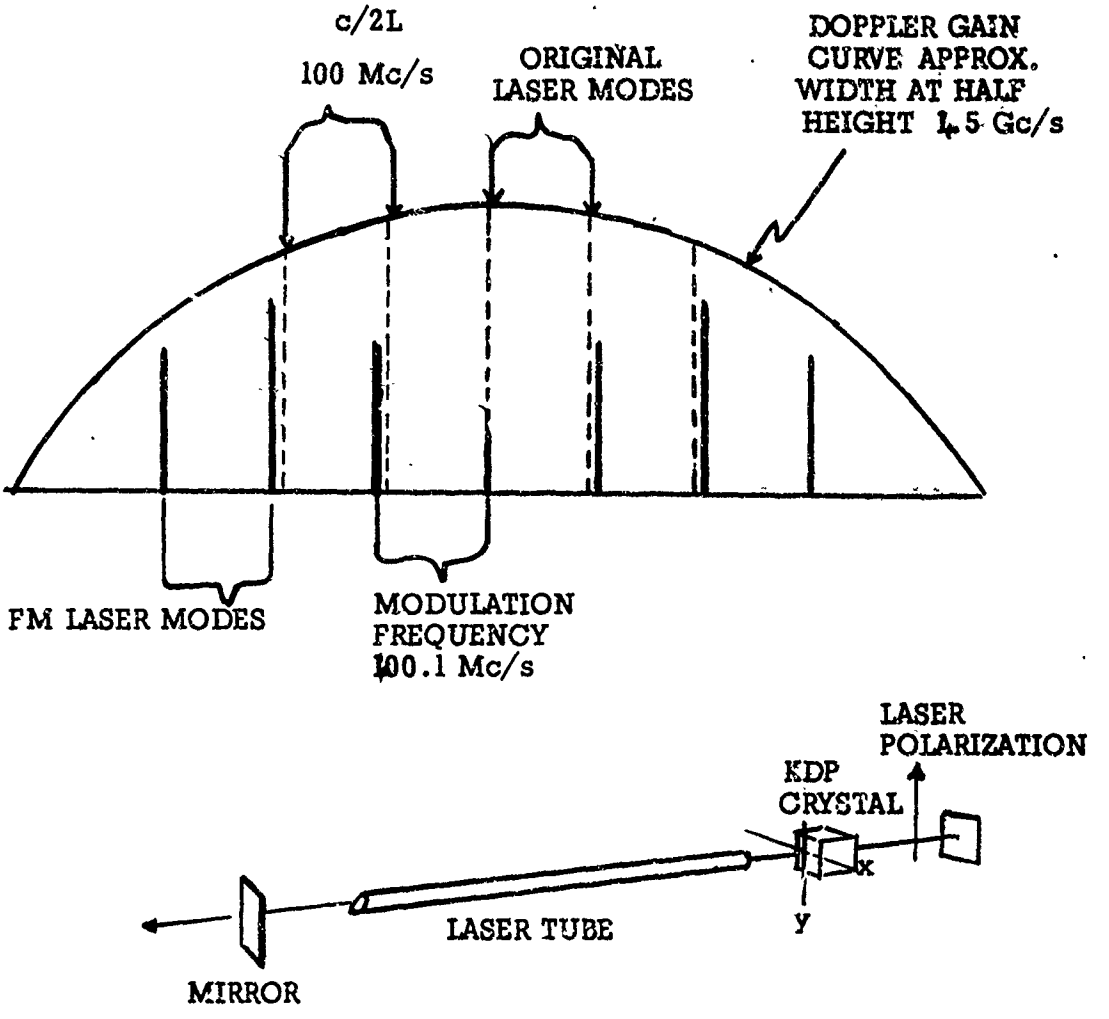

Fig. 30 A diagram of the spectrum of the FM Laser modes and the orientation of the internal modulator with respect to the laser polarization.

similar FM Laser mode spectrum actually obtained.

Harris and Targ made use of a scanning interferometer to observe the output spectrum of the original FM Laser. However the resolution of their instrument was inadequate for accurate experimental analysis. The SFPI was therefore constructed to provide approximately ten to one improvement in resolution which was necessary for analysis requirements in this program. Experimental application and results, including high resolution photographs of the laser output during subsequent FM Laser experimentation, are presented in the following part of this section.

D. Results of the experimental application of the scanning interferometer

Fig. 32 shows a schemetic of the arrangement of experimental apparatus used in the generation and study the FM Laser. Operation of the equipment was essentially the same as originally described by Harris and Targ as summarized in Section 7 C. The SFPI was aligned according to procedures described in Section 4 B.[15] Matching to the Spectra Physics model 116 laser was accomplished according to procedures described in Section 3 C for Case I. The specific matching graphs presented in Section 3 D were used to save considerable calculation and time for this matching situation. Actual matching values are included in Table II, Appendix I.

[15]Alignment was greatly facilitated by operating the laser in an AM locked condition, which gave a much more stable and clear display of the laser modes. Any interfering off-axis distortion was readily discernable and easily eliminated by alignment control adjustment.

Photographs of oscilliscope displays were obtained during experimentation with the FM Laser with the laser operating under various stages of mode control by the internal modulator. The improvement in resolution of the SFPI constructed over the previously available interferometer is clearly apparant from a comparison of Figs. 31-(I) and 31-(II) which show free running and FM Laser output spectra as viewed using the SFPI (I) and the previous interferometer (II). A typical display of the unstable free running laser modes is shown in Fig. 33a, and Fig. 33f shows the AM locked laser mode spectrum. Modulation depth Γ is varied to obtain various stages of the FM Laser as shown in Figs. 33b through e. A typical transition sequence from the AM locked condition to the FM Laser operation is shown in Fig. 34. This transition is dependent on the amount of detuning from the synchronous frequency, i. e., the axial mode spacing $c/2L$. Starting in the AM locked position , the modulator frequency is detuned slowly and the display observed on the oscilliscope until the FM Laser operation desired is achieved. In Fig. 35 the FM Laser operation is approached from the free running state by tuning the modulator towards the synchronous frequency

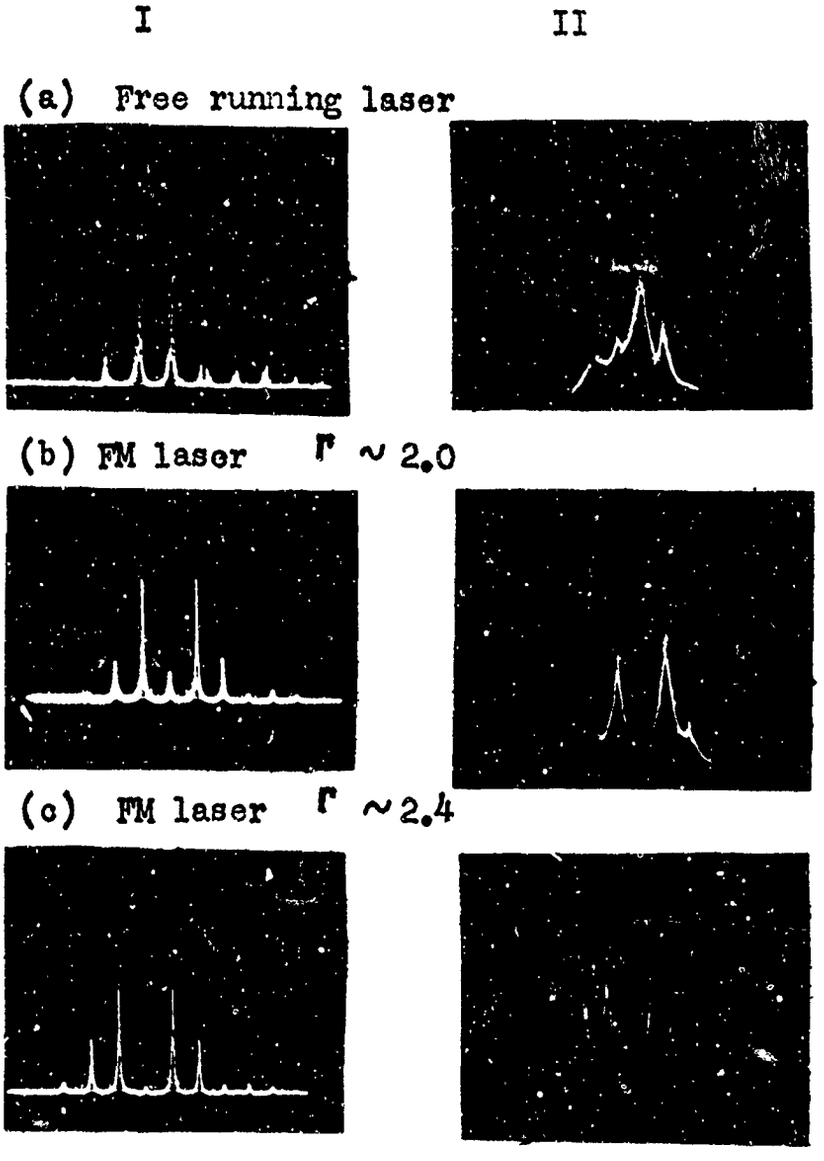

Fig. 31 Comparison of improved resolution in spectral analysis of SFPI (I) with previous observations by Harris and Targ (II)

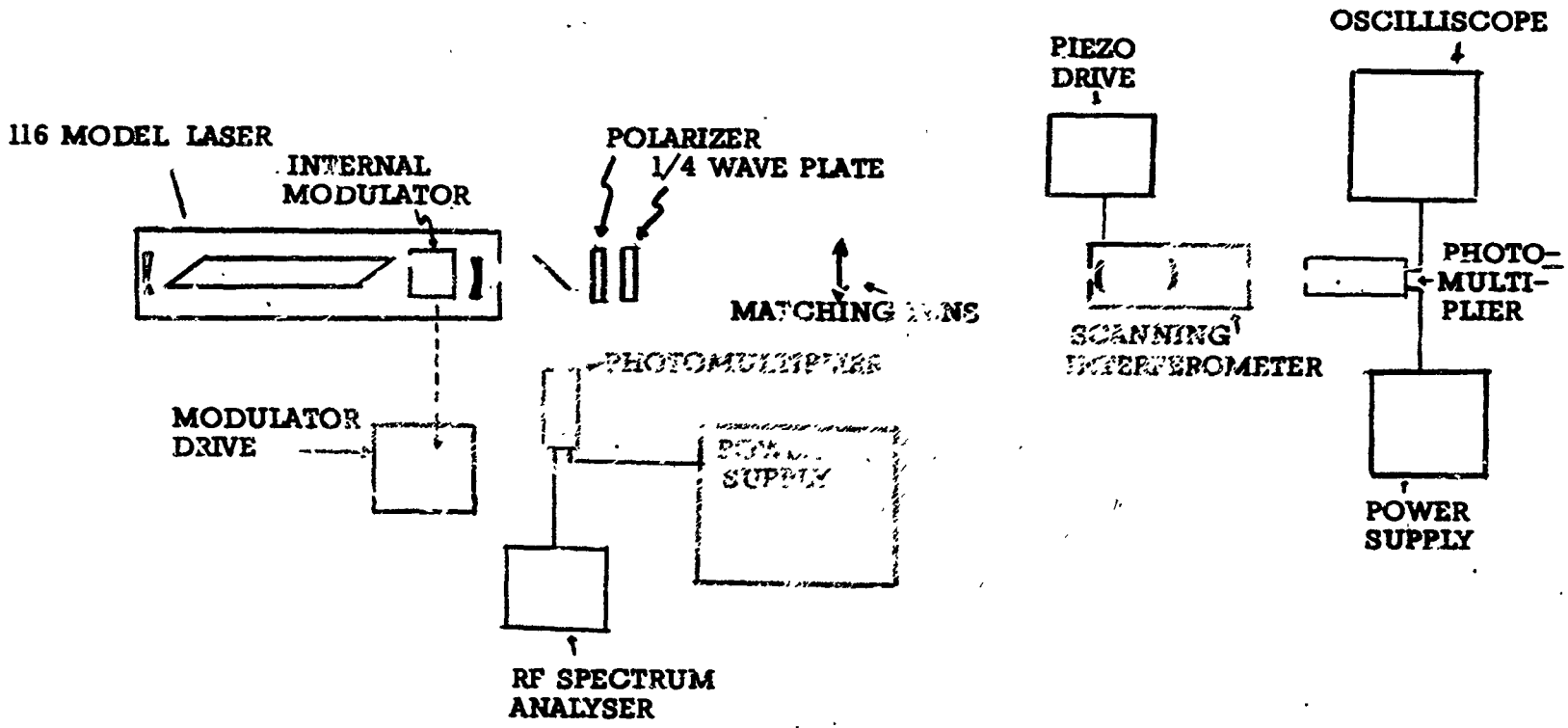

Fig. 32 A schematic arrangement of apparatus required for the generation and study of the FM Laser.

and observing the laser outpu spectrum stabilize and the amplitudes and phases of the modes take various FM sideband characteristics which depend on the amount of detuning and the power input to the modulator. Continuing to tune the modulator toward the synchronous frequency would eventually achieve the AM locked condition at a point near the synchronous frequency as determined by the laser power and the amount of detuning.

Similar high resolution photographs of the FM laser output spectra are now being obtained with the SFPI in the FM Laser program for detailed study and analysis of the effects of the various degrees of internal phase perturbation on the laser output spectrum characteristics.

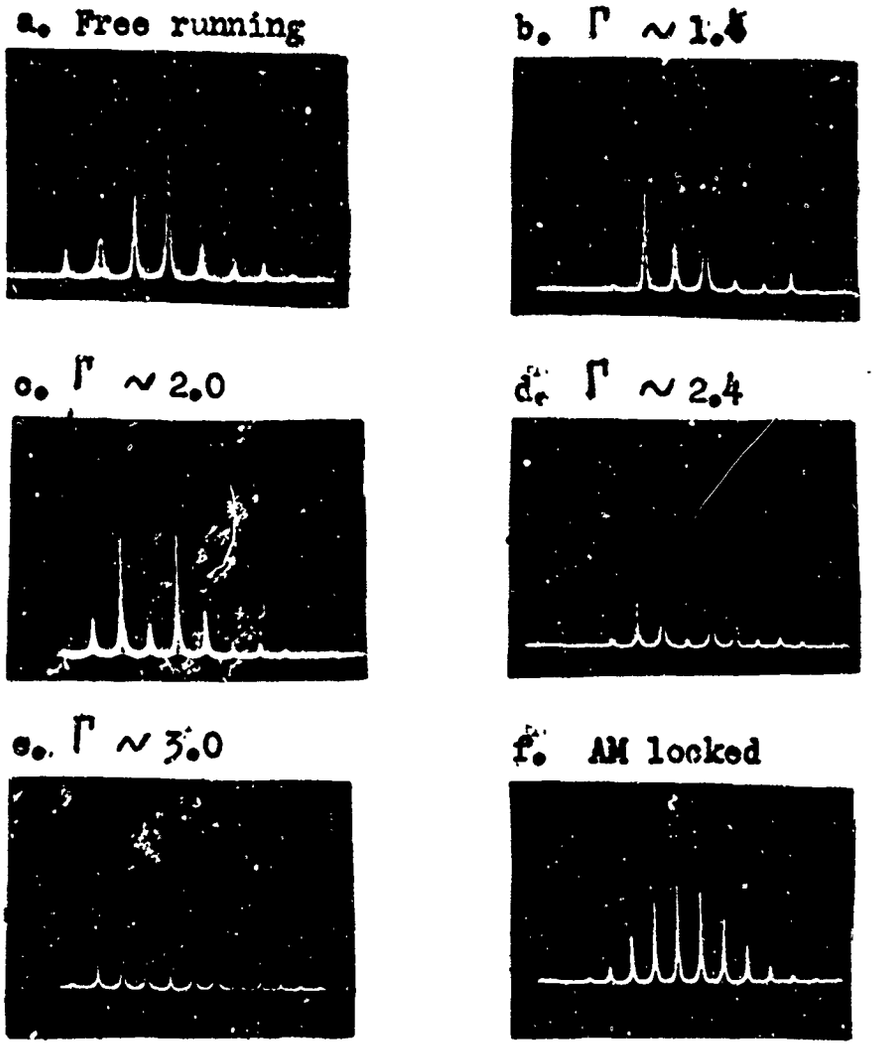

Fig. 33 Variation in laser output spectrum with change in modulation depth. Center mode amplitude assigned by $J_0(\Gamma)$ in typical FM distribution

Fig. 34 Transition from FM to AM locked laser with variation in modulator frequency

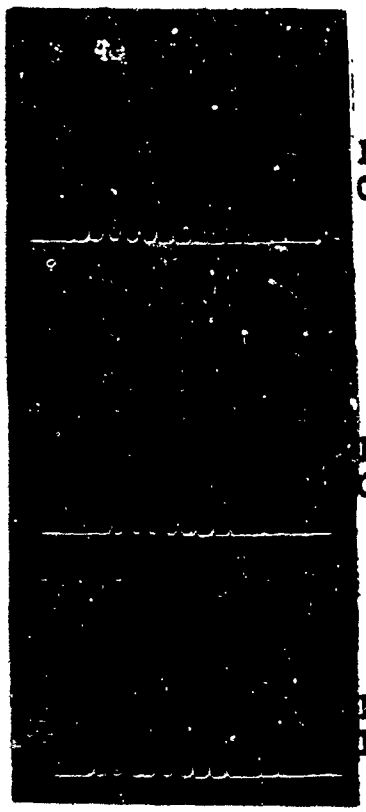

Fig. 35 Transition from free running to FM laser caused by a change in modulation depth Γ as modulator power input varies

8. Summary and Conclusions

A scanning Fabry Perot interferometer was constructed and evaluated as a high resolution instrument for spectrum analysis of laser radiation. Half-intensity widths of the transmitted light were observed as low as 5Mc, and practical application observations show better than ten to one improvement over previous measurements in the programs studied. Matching curves and outlined procedures for their use were verified by the many successful applications achieved. Working with the SFPI was directly a means of studying various laser outputs for greater variety and experience. Four different types of lasers were studied, and the knowledge and experience gained was far beyond expectations. A brief amount of time studying the stability characteristics of the laser gave insight and appreciation for the problems always encountered with practical laser experimentation. Additional time might well have been spent analyzing short term instabilities, but the FM laser program offered a great deal more value and interest, as well as need for the application of the SFPI. The results obtained while applying the SFPI to study the FM laser spectral characteristics were the most significant accomplishment of this project, and best representation of the value of the SFPI to state of the art experimentation.

The SFPI will continue to be useful in the FM program for additional study including such fundamental properties as frequency and amplitude stability, efficiency, and ever more important, in the development of the Super Mode laser concept [11]. The Super Mode laser is the result of a direct application of the FM laser to achieve high power single fre-

quency light by modulating the FM laser output externally with the same signal, exactly 180° out of phase, as applied to the internal modulator. The high resolution SFPI will give a clear indication of the various effects of the external modulation as attempt is made to achieve Super mode.

Thus to realize the full potential of the laser, its characteristics must be carefully studied and methods of accurate control exploited to fullest advantage and capability. The FM laser and the Super mode laser are excellent examples of state of the art efforts in just that direction. A signifi[illegible] role in the studies of laser radiation is filled by such instruments as a high resolution SFPI, which also by design utilizes the very same type of resonant cavity principles which originally contributed to the successful accomplishment of light amplification. The inherent characteristics of the laser give great promise, but greater still is the amount of research and study required to achieve an efficient, effective optical communications system.

Appendix I Summary of Matching Values

Matching measurements and results are summarized for the experimental applications of the SFPI during the project. Table I contains data for the Spectra Physics models 131 and 115 laser applications where the laser resonators were himispherical, i.e. Cases II and III as indicated. For this cases the characteristic matching length parameter f_0 becomes d_2, and d_1 is necessarily zero. Table II indicates the data for the FM laser application with the Spectra Physics model 116 laser operating with a spherical resonator, i.e., Case I. Variations in power and laser mirror separations will effect the output beam diameter and the subsequent matching values, so that check of the output spot size is recommended prior to following the data listed below.

TABLE I

Laser/Case Power output	w_1	L_I	Z_I	f_0
131/ Case II				
0.5 mw	.6 mm	5 cm	1.16 cm	.697 m
	.6 mm	7 cm	1.26 cm	.755 m
	.6 mm	11 cm	1.4 cm	.84 m
	.6 mm	14 cm	1.47 cm	.884 m
115/Case II				
1.7 mw	1.25 mm	7 cm	1.26 cm	1.59 m
2.8 mw	1.5 mm	7 cm	1.26 cm	1.9 m
115/ Case III				
0.05 mw	.4 mm	7 cm	1.26 cm	.5 m

TABLE II

	w_1	w_2	L_L	L_I	Z_L	Z_I	f_o	f	d_1	d_2
116/Case I	.46mm	.254mm	1.5m	7 cm	.85m	1.26cm	.59m	1.019m	2.2m	1.38m

Appendix II

Discussion of the operation of the CW He-Ne gas laser

Continuous laser oscillation is obtained from an electrical discharge within a plasma tube containing a mixture of Helium and Neon gases. Population inversion of energy levels in the Ne atomic system results in stimulated emission of radiation at 6328 A° wavelength within a high Q optical resonator consisting of the plasma tube located between two highly reflective dielectric coated mirrors in the configuration of a Fabry-Perot etalon. (See Fig. 36) The simplified energy level diagram in Fig. 37 shows the atomic energy levels and the inversion cycle involved in the production of coherent oscillation at the 6328 A° wavelength. Helium atoms are energized by external excitation (DC and or RF) to a metastable energy level of 20.61

Collision occurs between these energized He atoms and Ne atoms lying at the ground energy level. The Ne atoms thus become energized to the $^3S_2$ level (20.66 ev), eventually causing a population inversion at the Ne $^3S_2$ level relative to the $^2P_4$ level. Upon returning to ground, the $^3S_2$ level Ne atom omits a photon at 6328 A° wavelength which in turn will stimulate additional emission or downward transitions of a similar energy exchange. Photons traveling along the axis of the resonator are captured or reflected back into the system to continue to stimulate additional radiation which is of the same wavelength and phase. When the energy gain due to excitation is equal to or greater than losses due to reflection, diffraction, and transmission, the wave is reinforced and oscillations oc-

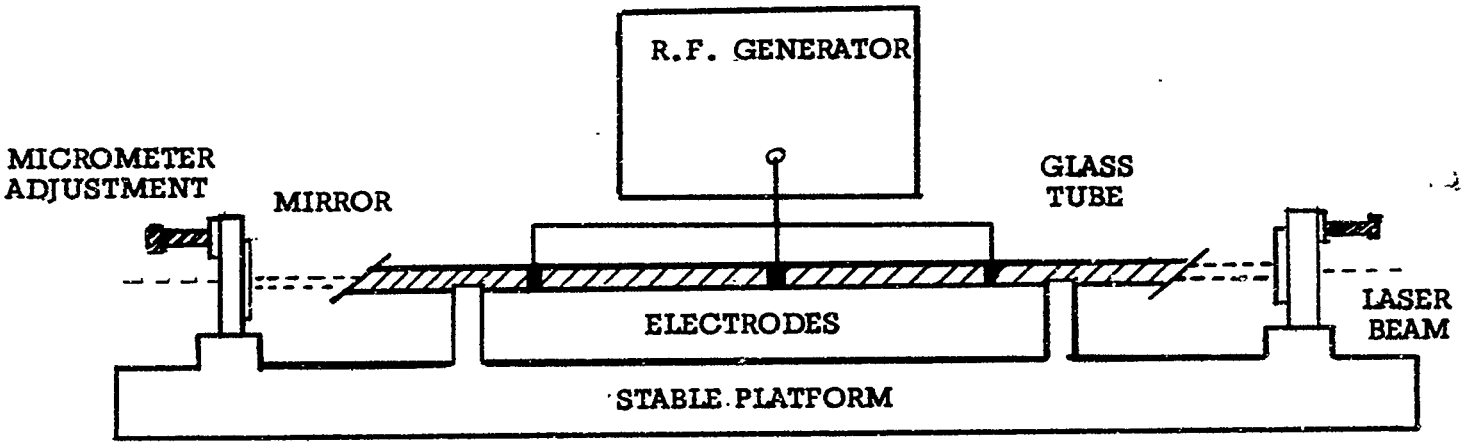

Fig. 36 A typical gas laser configuration

cur. A small portion of the radiation is transmitted through the 99% reflector and constitutes the useful multi-frequency laser beam available for study, or application as required.

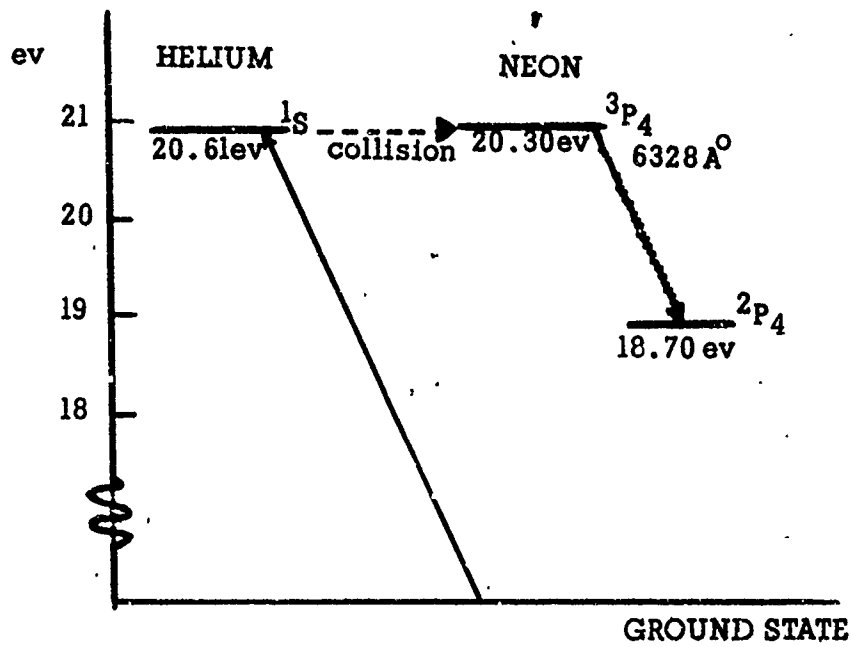

Fig. 37 A diagram of the Helium-Neon energy levels, electron volts, for the 6328 A° transition.

BIBLIOGRAPHY

1. Schalow, A. L. and C. H. Townes, Infrared and Optical Masers, Physical Review, v. 112, Dec. 1958: 1940.

2. Javan, A., et. al., Population Inversion and Continuous Optical Maser Oscillation in a Gas Discharge Containing a He-Ne Mixture, Physical Review Letters, v. 6, Feb. 1961: 106.

3. See for instance: Lengyel, B., Lasers, John Wiley & Sons, Inc. April, 1963: 101, 102.

4. Fox, A. and T. Li, Resonant Modes in a Maser Interferometer Bell Systems Technical journal, v. 40, March, 1961: 453-488.

5. Boyd, G. D. and J. P. Gordon, Confocal Multimode Resonator for Millimeter Through Optical Wavelength Masers, Bell Systems Technical Journal, v. 40, March, 1961: 489-508.

6. Boyd, G. D. and H. Kogelnik, Generalized Confocal Resonator Theory, Bell Systems Technical Journal, v. 41, July, 1962: 1368.

7. Siegman, A. E., et. al., Optical Heterodyning and Optical Demodulation at Microwave Frequencies; Symposium on Optical Masers, Polytechnic Institute of Brooklyn, April, 1960.

8. Targ, R. Optical Heterodyne Detection of Microwave Modulated Light, Proceedings IEEE(correspondence), v. 52, March, 1964: 303-304.

9. Harris, S. E. and R. Targ, FM Oscillations of the He-Ne Laser, Applied Physics Letters, v. 5, Nov. 1964: 202-204.

10. Harris, S. E. and O. P. McDuff, FM Laser Oscillation - Theory, Applied Physics Letters, v. 5, Nov. 1964: 204-206.

11. Massey, G. et. al., Generation of Single Frequency Light Using the FM Laser, Applied Physics Letters, v. 6, Jan. 1965: 10-11.

12. Targ, R. et. al., Light Modulation Detector, Interim Engineering Report No. 3, Technical Memorandum EDL-M811, Electronic Defense Labratories, Sylvania Electronics Systems (West), Mountain View, Calif., Jan. 1965.

13. Tolansky, S. and D. J. Bradley, Symposium on Interferometry HMSO, London, 1959: 375.

14. Connes, P., L' Etalon De Fabry-Perot Spherique Le Journal De Physique et Le Radium v. 19, March 1958: 262-269

15. Fork, R. L., et.al., A Scanning Spherical Mirror Interferometer for Spectral Analysis of Laser Radiation, Applied Optics, v. 3, Dec. 1964: 1471-1484

16. Forrester, A. et.al., Photoelectric Mixing as a Spectroscopic Tool, Journal Optical Society of America, v. 51, March 1961: 253-259

17. Born, M. and E. Wolf, Principles of Optics, Second Edition, Pergamon, 1964.

18. See for instance: Jenkins, F. A., and White, H. E. Fundamentals of Optics, Third edition, McGraw-Hill Co. Inc., 1957

19. Herriot, D., et.al., Off Axis Paths in Spherical Mirror Interferometers, Applied Optics, v. 3, April 1964: 523

20. Kogelnik, H. Matching of Optical Modes, Bell Systems Technical Journal, v. 44, Jan. 1964: 335-337.

21. Yariv, A., The Laser, Proceedings IEEE, v. 51, Jan. 1963: 4

22. Berlincourt, D. et. al., Transducer Properties of Lead Titanate Zirconate Ceramics, Proceedings IRE, v. 48, Feb 1960: 220-229.

23. Herriot, D. R., Optical Properties of a Continuous Helium Neon Optical Maser, Journel Optical Society of America, v. 52, Jan. 1962: 31-37.

24. Heinemann, H. M. and H. W. Redlien jr., The Observation of Mode Impurity in Gas Lasers Apparantly Resonating in the TEM-00 Mode, Proceedings IEEE, v. 53, Jan. 1965: 77-78.

25. Javan, A. et. al., Frequency Stability of He-Ne Lasers and Measurements of Length, Physical Review Letters, v. 10, March 1961: 163-167.

26. Harris, S. E., Conversion of FM light to AM Light Using Birefringent Crystals, Applied Physics Letters, v. 2, Feb. 1963: 47

27. Hargrove, L. E., Locking of the He-Ne Modes Induced by Synchronous Intracavity Modulation, Applied Physics Letters, v. 5, July 1964: 4

28. DiDomenico, M. D. jr., Small Signal Analysis of Internal (Coupling Type) Modulation of Lasers, Journal Applied Physics, v. 35, Oct. 1964:

29. Bennet, W. R. jr., Hole Burning Effects of the He-Ne Optical Maser, Physical Review, v. 126, April 1962: 580-593.

30. See for instance: Swartz, M., Information Transmission, Modulation, and Noise, McGraw-Hill Co. Inc., 1959